# Paleoclimate, paleoweathering and paleoredox conditions of Lower Cretaceous shales from the Mural Limestone, Tuape section, northern Sonora, Mexico: Constraints from clay mineralogy and geochemistry

**Jayagopal Madhavaraju[1,*], Erik Ramírez-Montoya[2], Rogelio Monreal[2], Carlos M. González–León[1], Teresa Pi-Puig[3], Inocente G. Espinoza-Maldonado[2], and Francisco J. Grijalva–Noriega[2]**

*[1] Estación Regional del Noroeste, Instituto de Geología, Universidad Nacional Autónoma de México, Hermosillo, Sonora 83000, Mexico.*
*[2] Departamento de Geología, Universidad de Sonora, Hermosillo, Sonora 83000, Mexico.*
*[3] Instituto de Geología, Universidad Nacional Autónoma de México,Ciudad Universitaria, 04510, Ciudad de México, Mexico.*
** mj@geologia.unam.mx*

**ABSTRACT**

Clay mineral analysis and major, trace and rare earth elements (REE) data were used in this study to interpret the paleoclimatic changes, paleoweathering and paleo-redox conditions in shale beds of the Tuape section of the Mural Limestone of Sonora. The clay mineralogical assemblages (illite-chlorite-kaolinite-smectite) of this section have provided information on the climatic conditions and environment of deposition that prevailed during late Aptian-early Albian age. The chondrite-normalized REE patterns are characterized by enriched LREE, flat HREE with negative Eu anomaly. The chemical index of alteration (CIA) and plagioclase index of alteration (PIA) values for these shales and A-CN-K diagram indicate a moderate intensity of chemical weathering. The low contents of TOC, TN, Mo, U and V and low Ni/Co and U/Th ratios in the Cerro La Ceja, Los Coyotes and Mesa Quemada members suggest that they have been deposited under oxic conditions. However, the Tuape Shale and Cerro La Puerta members show relatively low to moderate contents of redox sensitive elements, and their ratios suggest that the depositional basin experienced oxic to anoxic depositional conditions.

Key words: geochemistry; clay mineralogy; paleoclimate; paleoweathering; paleo-redox conditions; Mural Limestone; Sonora.

**RESUMEN**

*Se realizaron análisis de arcillas minerales, elementos mayores, traza y tierras raras (ETR) para interpretar los cambios paleoclimáticos, el paleointemperismo y las condiciones de paleo-reducción-oxidación en las capas de lutita de la sección Tuape de la Caliza Mural de Sonora. La asociación mineralógica de arcillas (ilita-clorita-caolinita-esmectita) de la sección Tuape proporcionó información sobre las condiciones climáticas y ambientes de depósito que predominaron durante el Aptiano tardío-Albiano temprano. Los patrones de tierras raras normalizados con condrita están caracterizados por el enriquecimiento de tierras raras ligeras (ETRL) y la disminución de tierras raras pesadas (ETRP) con anomalía negativa de Eu. Los valores del índice de alteración química (CIA por sus siglas en inglés) y del índice de alteración de plagioclasas (PIA por sus siglas en inglés) para estas lutitas así como el diagrama A-CN-K, indican que su intemperismo químico es de una intensidad moderada. Los bajos contenidos de carbono orgánico total (COT), nitrógeno total (NT), Mo y V, además de la baja relación Ni/Co y U/Th en los miembros Cerro La Ceja, Los Coyotes y Mesa Quemada sugieren que se depositaron bajo condiciones óxicas. Sin embargo, los miembros Lutita Tuape y Cerro La Puerta muestran contenidos relativamente bajos a moderados de elementos sensibles a reducción-oxidación y sus relaciones sugieren que la cuenca de depósito experimentó condiciones de depósito de óxicas a anóxicas.*

*Palabras clave: geoquímica; mineralogía de arcillas; paleoclima; paleointemperismo; condiciones de paleo-reducción-oxidación; Caliza Mural; Sonora.*

## INTRODUCTION

The chemical composition of shales provides important information on regional tectonic setting, provenance, weathering conditions, and sediment recycling (Roser and Korsch, 1988; McLennan *et al*., 1993; Cullers, 1995). The geochemistry of fine-grained sediments, in particular trace elements, is believed to represent the average composition of the upper continental crust more than any other sedimentary rocks (DaPeng *et al*., 2012), as they preserve the provenance signature and diagenetic history (Baioumy and Ismael, 2010; Mondal *et al*., 2012; Spalletti *et al*., 2012). In fact, the geochemical composition of clastic sediments is a complex function of variables such as source material, weathering, physical sorting, and diagenesis (Nagarajan *et al*., 2007a, 2007b; Moosavirad *et al*., 2012; Armstrong-Altrin *et al*., 2013, 2015; Madhavaraju, 2015). However, many studies proved that the geochemical composition of clastic sediments are useful to understand the source-area weathering conditions (Selvaraj and Chen, 2006; Gupta *et al*., 2012; Raza *et al*., 2012) and provenance (Cullers, 2000, 2002; Armstrong-Altrin, 2009; Fatima and Khan, 2012; Madhavaraju, 2015; Ramachandran *et al*., 2016). Likewise, certain trace elements and their ratios and REE patterns of the clastic sediments are believed to be an effective tool for the reconstruction of source rock composition because they are not significantly redistributed in the course of sedimentation, lithogenesis, and metamorphism (Fu *et al*., 2010; Etemad-Saeed *et al*., 2011; Zaid, 2012).

Madhavaraju, J., Ramírez-Montoya, E., Monreal, R., González–León, C.M., Pi-Puig, T., Espinoza-Maldonado, I.G., Grijalva–Noriega, F.J., 2016, Paleoclimate, paleoweathering and paleoredox conditions of Lower Cretaceous shales from the Mural Limestone, Tuape section, northern Sonora, Mexico: Constraints from clay mineralogy and geochemistry: Revista Mexicana de Ciencias Geológicas, v. 33, núm. 1, p. 34-48.

Certain elements actively participate in various geochemical processes taking place in marine environments and they may become authigenically enriched or depleted in sediments depending on the availability of free oxygen during deposition; as a result, the distribution patterns of such elements are extensively used to understand the variations in paleo-redox conditions in both modern marine sediments and ancient rocks (Calvert and Pedersen, 1993; Canet *et al*., 2004; Algeo and Maynard, 2004; Tribovillard *et al*., 2006; Nagarajan *et al*., 2007b; Madhavaraju and Lee, 2009; Madhavaraju *et al*., 2015a).

The clay mineralogical composition of sediments can reflect the effects of several paleoenvironmental conditions (climate, sea level fluctuations, tectonic activity as well as continental and basin morphology). The clay minerals study is considered to be a powerful tool for the interpretation of weathering conditions and paleoclimate in the source area (Chamley, 1989; Madhavaraju and Ramasamy, 2001; Madhavaraju *et al*., 2002; Ruffell *et al*., 2002; Ahlberg *et al*., 2003; Deconinck *et al*., 2005; Dera *et al*., 2009).

For the present study, shale samples were collected from the exposed section of the Mural Limestone located near the town of Tuape, northern Sonora. Major, trace and rare earth elements, and clay minerals were analyzed from samples collected at several stratigraphic level of this section. The purpose of the present study is to identify the paleoclimatic changes recorded in the shale sequences, to assess the intensity of source area weathering, and to infer paleo-redox conditions in the Tuape section of the Mural Limestone.

## GEOLOGY OF THE STUDY AREA

The Lower Cretaceous Mural Limestone, well exposed in northern Sonora, Mexico (Figure 1), was deposited on a shallow marine platform during Aptian-Albian time (Scott, 1987). These sedimentary rocks show similar stratigraphic characteristics and are correlative with rocks exposed in southern Arizona and New Mexico in the United States of America (Ransome, 1904; Cantú-Chapa, 1976; Bilodeau and Lindberg, 1983; Mack *et al*., 1986; Dickinson *et al*., 1989; Jacques-Ayala, 1995; Lawton *et al*., 2004). Various geochemical and isotopic studies have been undertaken on the carbonate rocks of the Mural Limestone to understand their depositional and diagenetic environments (Madhavaraju *et al*., 2010; Madhavaraju and González-León, 2012; Madhavaraju *et al*., 2013a, 2013b; 2015b). Regionally, the Mural Limestone overlies and underlies thick fluvial successions consisting of reddish brown sandstone, siltstone and conglomerate of the Morita and Cintura Formations, respectively. In addition to that, the Glance Conglomerate that underlies the Morita Formation is composed of cobble- to boulder-conglomerate with local interbeds of volcanic flows and tuffs. These formations together compose the Bisbee Group which represent syntectonic rift deposits that were deposited in the Bisbee basin of northern Sonora and southeastern Arizona (Bilodeau *et al*., 1987; Lawton *et al*., 2004). Mural Limestone has been divided into six members in Sonora by Lawton *et al.* (2004): Cerro La Ceja (CLC), Tuape Shale (TS), Los Coyotes (LC), Cerro La Puerta (CLP), Cerro La Espina (CLE) and Mesa Quemada (MQ) members.


Figure 1. Location map of the Mural Formation in the Tuape area.

The Tuape section spans from the basal Cerro La Ceja to the Mesa Quemada members at the top of the Mural Limestone (Figure 2) (Lawton *et al*., 2004; González-León *et al.,* 2008; Ramírez-Montoya, 2014 ). The CLC Member consists of bioclastic limestone, sandstone, siltstone and shale. The limestone beds are grey, brown and dark yellowish brown, and locally sandy. Siltstone beds are grey, green and reddish brown with calcareous nodules. Shale beds are brown and green and locally contain silty materials. The TS Member is mainly composed of grey to black shale, shaly limestone and subordinate amount of siltstone and fine-grained sandstone. Limestone occurs as thin beds which contain oysters and ammonites. The LC Member consists of thin beds of brown shale, calcareous siltstone, shaly limestone, massive brown siltstone, fine-grained sandstone and bioclastic limestone. The CLP Member is mainly composed of black shale and thin beds of fine-grained sandstone and fossiliferous limestone. The CLE Member is composed mostly of massive limestone with thin beds of siltstone, mudstone, fine-grained sandstone and shaly limestone. The MQ Member includes green shale, light grey to red siltstone, sandstone and bioclastic limestone. Earlier studies confirmed that the Mural Limestone ranges from late Aptian to early Albian (Lawton *et al.,* 2004; González-León *et al.,* 2008; Madhavaraju *et al*., 2013b).

## MATERIALS AND METHODS

Twenty one samples were selected for major, trace and rare-earth elements geochemistry. Major, trace and rare earth elements concentrations were analyzed at Instituto de Geología, Universidad Nacional Autónoma de México, México. Each collected sample was powdered in an agate mortar, and fused-glass beads were prepared for major elements analysis. Major elements composition was obtained by X-ray fluorescence in fused $LiBO_2/Li_2B_4O_7$ disks using a Siemens SRS-3000 X-ray fluorescence spectrometer with an Rh-anode X-ray tube as a radiation source. X-ray absorption/enhancement effects were corrected using the Lachance and Traill (1966) method, included in the SRS-3000 software. The geochemical standard JGB1 (GSJ) was used to determine data quality (Table 1). The analytical accuracy errors were better than ±2% for $SiO_2$, $Fe_2O_3$, CaO and $TiO_2$ (1.15%, 0.66%, 1.43%, 0.63, respectively) and better than ±5% for $Al_2O_3$, MgO, $Na_2O$ and $K_2O$ (3.32%, 3.57%, 4.17%, 4.17%, respectively). The accuracy errors of MnO and $P_2O_5$ were more than ±5% (5.26%, 7.14%, respectively). One gram of sample was heated to 1000 ºC in porcelain crucibles for one hour to measure the loss on ignition (LOI).

Trace and rare earth elements were determined by an Agilent 7500 ce Inductively Coupled Plasma Mass Spectrometer (ICP-MS)

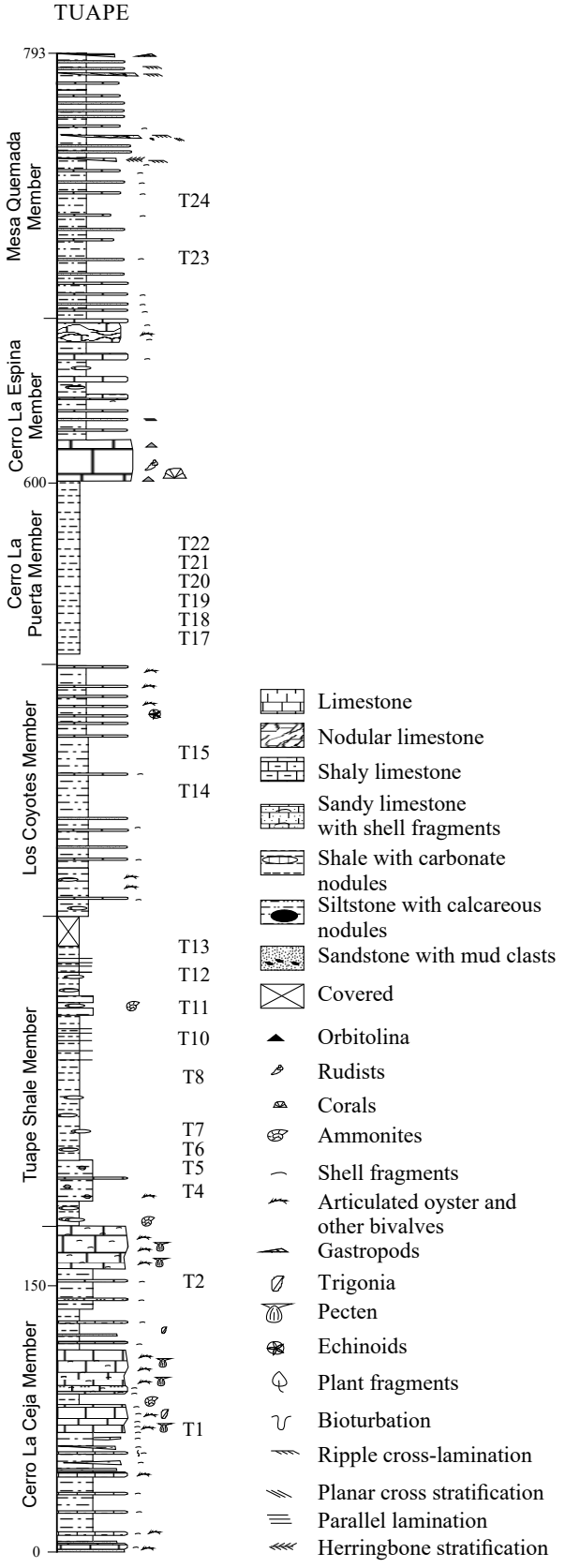


Figure 2. Lithostratigraphic section of the Mural Limestone in Tuape (modified after Lawton *et al.*, 2004). T1-T24 indicate stratigraphic position of the shale samples collected in the present study.

Table 1. Comparison of major oxide data for GSJ reference sample JBG1 with GSJ certificate of analysis data (Imai *et al.*, 1995) as well as limits of detection (LOD) data for XRF analyses.

| Oxide/Elements | This Study* | Literature value | LOD** |
|---|---|---|---|
| $SiO_2$ | 43.16 | 43.66 | 0.050 |
| $Al_2O_3$ | 16.91 | 17.49 | 0.018 |
| $Fe_2O_3$ | 15.16 | 15.06 | 0.006 |
| CaO | 11.73 | 11.90 | 0.040 |
| MgO | 7.57 | 7.85 | 0.015 |
| $K_2O$ | 0.23 | 0.24 | 0.030 |
| $Na_2O$ | 1.15 | 1.20 | 0.050 |
| MnO | 0.18 | 0.19 | 0.004 |
| $TiO_2$ | 1.59 | 1.60 | 0.004 |
| $P_2O_5$ | 0.06 | 0.056 | 0.004 |
| LOI | - | - | - |

* Major elements in wt % are by XRF. ** LOD (limit of detection) in wt%.
- : not determined or not reported.

according to standard analytical procedures suggested by Eggins *et al.* (1997). The analytical results for the IGLa-1 and GSR2 obtained in the present study were compared with the published values (Table 2) reported by Govindaraju (1994) that allowed to improve the quality and accuracy of the analysis. The analytical precision errors for Ba, Cr, Sc, V, Y, Sr, Zr, Nb and Rb were better than ±4%, while for Co, Zn and Pb were better than ±6%. The analytical accuracy errors of certain trace elements (Cu, Ni, Th and U) were better than ±10%.

The accuracy errors for rare earth elements such as La, Ce, Pr, Nd, Sm, Dy, Ho, Er and Lu were better than ±4%, and, Eu, Gd, Tb, Tm and Yb were better than ±10%. The detection limits for the instrument used in this study are given in Table 2. They generally obey the findings suggested by Verma *et al.* (2002), Santoyo and Verma (2003), and Verma and Santoyo (2005). Rare earth elements were normalized to chondrite values of Taylor and McLennan (1985) for preparing REE-normalized diagrams. The Eu/Eu* (Eu anomaly) is calculated using the value of Eu ($Eu_{sample}/Eu_{chondrite}$) and the predicted value of Eu* is obtained from the interpolation from the chondrite - normalized values of Sm and Gd.

Twelve samples were selected for the clay minerals study. Samples were prepared following standard XRD procedures (Brindley and Brown, 1980; Moore and Reynolds, 1989). For whole-rock mineralogy analysis samples were ground with an agate pestle and mortar to <75 μm and mounted in aluminum holders for X-ray powder diffraction analysis. For clay mineral analysis, the <2 μm fraction was separated by gravity settling, washed and concentrated by centrifugation and prepared for X-ray diffraction (XRD) by sedimentation onto round glass slides. Measurements were made using a Shimadzu XRD-6000 diffractometer at Instituto de Geología, Universidad Nacional Autónoma de México, México. This equipment operated with an accelerating voltage of 40kV and a filament current of 30mA, using $CuK_\alpha$ radiation and graphite monochromator. Clay samples were examined by XRD in the air-dried form, saturated with ethylene glycol (EG) and after heating (550 °C). We compared patterns produced from air dried with EG solvated preparations. All the preparations were measured over a 2θ angle range of 2-70° (air-dried) and 2-40° (glycolated and heated) in steps of 0.02° and 2 seconds integration time. Profiles were analyzed using Shimadzu software. Peak positions ("d" spacings) were standardized against quartz 100 peak taken at 4.26 Å. To obtain statistically representative values, all samples were analyzed by duplicate. All the measurements were done under the same analytical conditions and calibrated using international reference materials (NIST 675 and NIST 640d). All values given here are of relative clay mineral abundance, *i.e.*, abundance of that particular clay mineral relative to the total clay mineral assemblage of a sample. Total organic carbon and total

Table 2. Comparison of data of trace and rare earth elements data for IGLa-1 and GSR2 reference samples.

| Oxide/ Elements | IGLa-1 | GSR2 | This study* | | LOD ** |
|---|---|---|---|---|---|
| | | | IGLa-1 | GSR2 | |
| Ba | 918.51 | 1,020 | 917.57 | 1,012.49 | 2.9712 |
| Co | 11.29 | 13.20 | 11.19 | 12.26 | 0.0213 |
| Cr | 29.21 | 33.40 | 28.63 | 32.16 | 2.4233 |
| Cu | 15.49 | - | 14.29 | 52.66 | 0.0290 |
| Zn | 78.75 | 71 | 75.90 | 66.24 | 1.4882 |
| Sc | 12.19 | 9.50 | 11.99 | 9.63 | 0.0472 |
| V | 97.97 | 95.50 | 102.02 | 96.62 | 1.3595 |
| Y | 27.25 | 9.30 | 27.85 | 9.37 | 0.1902 |
| Sr | 574.75 | 790 | 562 | 803.60 | 6.0714 |
| Zr | 241.93 | 99 | 248.53 | 94.36 | 4.3175 |
| Nb | 18.96 | 6.80 | 19.5 | 6.03 | 0.0102 |
| Ni | 8.38 | 17 | 7.21 | 18.47 | 0.5802 |
| Pb | 10.24 | 11.30 | 19.90 | 10.70 | 0.3249 |
| Rb | 32.77 | 37.60 | 32.23 | 38.13 | 0.4833 |
| Th | 2.97 | 2.90 | 2.96 | 2.42 | 0.0151 |
| U | 0.99 | 0.90 | 1.01 | 0.83 | 0.0217 |
| La | 28.96 | 21.80 | 29.15 | 21.65 | 0.0136 |
| Ce | 56.73 | 40.00 | 58.31 | 40.58 | 0.0351 |
| Pr | 7.13 | 4.90 | 7.29 | 4.66 | 0.0088 |
| Nd | 28.65 | 19.00 | 29.59 | 18.26 | 0.0107 |
| Sm | 6.13 | 3.40 | 6.05 | 3.34 | 0.0918 |
| Eu | 1.85 | 1.02 | 1.79 | 1.10 | 0.0435 |
| Gd | 5.96 | 2.70 | 5.67 | 3.03 | 0.0028 |
| Tb | 0.88 | 0.41 | 0.89 | 0.38 | 0.0535 |
| Dy | 4.87 | 1.80 | 4.77 | 1.78 | 0.1087 |
| Ho | 0.99 | 0.34 | 1.04 | 0.33 | 0.0070 |
| Er | 2.76 | 0.85 | 2.69 | 0.84 | 0.0360 |
| Tm | 0.39 | 0.15 | 0.40 | 0.13 | 0.0071 |
| Yb | 2.60 | 0.89 | 2.55 | 0.77 | 0.0605 |
| Lu | 0.41 | 0.12 | 0.38 | 0.11 | 0.0077 |

* Trace and rare earth elements in ppm by ICP-MS . ** LOD (limit of detection) in ppb. - : not determined or not reported.

nitrogen concentrations were analyzed using a CHNS 2400 series II Perkin Elmer elemental analyser at Instituto de Geología, Universidad Nacional Autónoma de México, México.

## RESULTS

### Clay mineralogy

The bulk mineralogy of the shales is listed in Table 3. The shales from the CLC Member (Figure 3) yielded the following results: illite (54%) and smectite (37%) are the commonest clay minerals whereas kaolinite (9%) is present in minor amount (Figure 3). The associated non-clay minerals observed in this member are quartz, feldspar, calcite and phyllosilicate. The TS Member is dominated by illite (40 – 70%) (Table 4). Larger fluctuations are observed in the chlorite (4 – 40%) and kaolinite (14 – 42%) contents. The chlorite content decreases towards the top of this member; kaolinite shows an increasing trend towards the top of the TS Member (Figure 3). The LC Member shows high content of chlorite (48%) and illite (39%) than kaolinite (13%). The CLP Member show large variations in chlorite (14 – 67%), illite (17 – 50%) and kaolinite (16 – 46%) contents. The MQ Member is dominated by both illite (30 – 46%) and chlorite (31 – 40%) followed by kaolinite (23 – 30%).

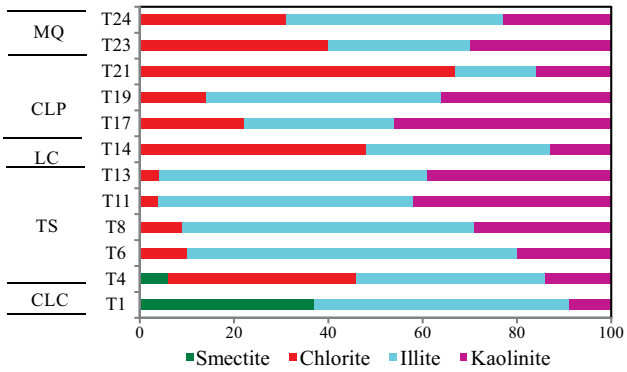


Figure 3. Clay mineralogical variations of shales from Tuape section of the Mural Limestone.

### Major elements

Slight enrichment of $SiO_2$ is noticed in CLC, LC and MQ members (61.2 – 62.5%; 61.0 – 61.8%; 62.3 – 65.1%; respectively) over TS and CLP members (53.6 – 61.0%; 52.6 – 57.7%; respectively). The content of $Al_2O_3$ is comparable in the five members of the Mural Limestone (CLC: 14.2 – 14.7%; TS: 11.7 – 15.5%; LC: 14.4 – 15.1%; CLP: 12.4 – 14.5%; MQ: 14.1 – 15.0%; respectively). TS and CLP members show higher concentration of CaO (2.77 – 11.47%: 5.81 – 10.51%; respectively) than CLC, LC and MQ members (3.26 – 3.70%; 3.36 – 3.84%; 2.17 – 2.88%; respectively). $K_2O$ contents are higher than $Na_2O$ in the studied shales (Table 5). Overall, the shale samples have low MgO, MnO, $TiO_2$ and $P_2O_5$ contents (Table 5).

The classification of the shale samples into mafic, intermediate and felsic compositions uses the calculated $(SiO_2)_{adj}$ values (Le Bas *et*

Table 3. Bulk mineralogy of the shales from Tuape section of the Mural Limestone.

| Sample No. | Quartz | Feldspars | Phillosilicates | Carbonate | Oxides | Apatite | Total |
|---|---|---|---|---|---|---|---|
| T1 | 32.7 | 20.9 | 31.9 | 9.7 | 4.9 | 0.0 | 100 |
| T4 | 31.2 | 23.2 | 30.1 | 9.2 | 5.7 | 0.3 | 100 |
| T6 | 26 | 25.3 | 24 | 20.4 | 4.3 | 0 | 100 |
| T8 | 25.9 | 26.0 | 22.0 | 20.1 | 3.4 | 0.2 | 100 |
| T11 | 25.8 | 29.0 | 30.3 | 10.4 | 4.4 | 0.2 | 100 |
| T13 | 28.0 | 31.4 | 24.4 | 10.4 | 5.1 | 0.1 | 100 |
| T14 | 28.2 | 32.3 | 24.3 | 10.0 | 5.3 | 0.0 | 100 |
| T17 | 27.2 | 27.0 | 24.9 | 15.8 | 5.1 | 0.0 | 100 |
| T19 | 30.8 | 25.1 | 20.6 | 18.6 | 4.8 | 0.0 | 100 |
| T21 | 30.6 | 28.1 | 20.2 | 15.3 | 4.9 | 0.2 | 100 |
| T23 | 29.4 | 29.3 | 21.5 | 14.8 | 4.9 | 0.1 | 100 |
| T24 | 27.6 | 27.3 | 22.8 | 17.2 | 5.0 | 0.1 | 100 |

Table 4. Clay minerals abundance in shales from Tuape section of the Mural Limestone.

| Sample No. | Illite | Clorite | Smectite | Kaolinite | Total |
|---|---|---|---|---|---|
| T1 | 54 | | 37 | 9 | 100 |
| T4 | 40 | 40 | 6 | 14 | 100 |
| T6 | 70 | 10 | | 20 | 100 |
| T8 | 62 | 9 | | 29 | 100 |
| T11 | 54 | 4 | | 42 | 100 |
| T13 | 57 | 4 | | 39 | 100 |
| T14 | 39 | 48 | | 13 | 100 |
| T17 | 32 | 22 | | 46 | 100 |
| T19 | 50 | 14 | | 36 | 100 |
| T21 | 17 | 67 | | 16 | 101 |
| T23 | 30 | 40 | | 30 | 100 |
| T24 | 46 | 31 | | 23 | 100 |

*al*., 1986). Such classification has been used by few workers (Hayashi *et al*., 1997; Armstrong-Altrin, 2009). Most of the samples fall in the felsic compositional field whereas few samples fall in the intermediate compositional field (Figure 4). The ratio $K_2O/Al_2O_3$ can be used as an indicator of the original composition of ancient mudrocks. $K_2O/Al_2O_3$ ratios for clay minerals (0.0 to 0.3) are markedly different from those for feldspars (0.3 to 0.9; Cox *et al*., 1995 ). In the present study, $K_2O/Al_2O_3$ ratios lie in the range of values for clay minerals, particularly between 0.13 and 0.21, which suggest that the clay minerals present in them are mostly of kaolinte and illite compositions.

**Trace elements**

The concentrations of trace elements of the shales are given in Table 6. The trace elements were normalized using North American Shale Composite values (NASC) (Gromet *et al*., 1984) and are plotted in a multi-element diagram (Figure 5). In comparison with NASC (Figure 5), CLC and TS members show similar concentration of Sr and Ba contents and slightly depleted in Rb content. LC and CLP members are slightly enriched in Sr content and slightly depleted in Rb and Ba with respect to NASC. In the MQ Member, the large-ion lithophile elements such as Rb and Ba show moderate depletion whereas Sr show slight depletion compared to NASC. The clear positive correlation observed between Rb and $K_2O$ (r = 0.81, n = 21) suggest that their distribution are mainly controlled by clay minerals. However, absence of such correlation observed between Ba and $K_2O$ (r = 0.32, n = 21) suggest that their distribution are not controlled by the clay minerals.

In NASC normalized diagram, most of the shales are depleted in high field strength elements (Zr, Hf, Y, Nb, Th and U). Few shales (T1 and T2) have similar concentration of Y with respect to NASC. Most of the shales from TS and CLP members are enriched in U compared to NASC. Positive correlation of $Al_2O_3$ with Nb and Y (r = 0.58; r = 0.54; respectively) reflects that these elements are probably hosted by clay minerals. In addition, Th shows strong correlation with $Al_2O_3$ (r = 0.65) implying that they may be controlled by clay minerals. Uranium contents show no correlation with $Al_2O_3$ content (r = -0.37), indicating that this element is not controlled by the clay minerals, but might be associated with other phases.

The shales are significantly depleted in Co content relative to NASC. Most of the shales show moderate depletion in Ni content compared to NASC. In comparison with NASC (Figure 5), shales show similar concentration of Sc. In CLC, TS and CLP members, the transition trace elements such as V and Cr show either slight depletion or slight enrichment whereas LC and MQ members show moderate depletion compared to NASC. The transition trace elements (V, Cr, Co and Ni) show no correlation with $Al_2O_3$ (r = 0.16; r = -0.43; r = 0.07, r = -0.30; respectively) which suggest that these elements were

Table 5. Concentration of major oxides (%) in shales from Tuape section of the Mural Limestone.

| Member/S. No. | $SiO_2$ | $Al_2O_3$ | $Fe_2O_3$ | CaO | MgO | $Na_2O$ | $K_2O$ | MnO | $TiO_2$ | $P_2O_5$ | LOI | Total | CIA | $Al_2O_3/TiO_2$ |
|---|---|---|---|---|---|---|---|---|---|---|---|---|---|---|
| *Mesa Quemada* | | | | | | | | | | | | | | |
| T23 | 62.3 | 14.1 | 6.50 | 2.88 | 3.02 | 1.72 | 1.81 | 0.02 | 0.87 | 0.20 | 6.34 | 99.77 | 59 | 20 |
| T24 | 65.1 | 15.0 | 4.94 | 2.17 | 2.46 | 2.29 | 2.46 | 0.02 | 0.76 | 0.16 | 4.57 | 99.87 | 65 | 16 |
| *Cerro La Puerta* | | | | | | | | | | | | | | |
| T22 | 57.7 | 13.5 | 5.57 | 7.29 | 1.85 | 1.72 | 2.31 | 0.03 | 0.66 | 0.10 | 9.21 | 99.95 | 62 | 21 |
| T21 | 55.4 | 12.8 | 5.04 | 9.16 | 2.07 | 1.89 | 2.12 | 0.05 | 0.65 | 0.11 | 10.37 | 99.72 | 60 | 20 |
| T20 | 56.6 | 14.5 | 5.77 | 5.81 | 2.65 | 1.40 | 2.69 | 0.04 | 0.67 | 0.14 | 8.57 | 98.84 | 66 | 22 |
| T19 | 56.9 | 13.7 | 5.98 | 6.22 | 2.42 | 1.52 | 2.39 | 0.04 | 0.68 | 0.14 | 8.71 | 98.76 | 64 | 20 |
| T18 | 52.6 | 12.4 | 4.71 | 10.51 | 2.04 | 1.76 | 2.12 | 0.05 | 0.62 | 0.12 | 11.70 | 98.68 | 61 | 20 |
| T17 | 55.9 | 14.0 | 6.30 | 6.72 | 2.59 | 1.44 | 2.45 | 0.05 | 0.69 | 0.13 | 9.06 | 99.31 | 65 | |
| *Los Coyotes* | | | | | | | | | | | | | | |
| T15 | 61.0 | 15.1 | 6.52 | 3.84 | 2.13 | 1.81 | 2.23 | 0.04 | 0.63 | 0.17 | 6.44 | 99.85 | 64 | 24 |
| T14 | 61.8 | 14.4 | 6.94 | 3.36 | 1.92 | 1.90 | 2.12 | 0.03 | 0.70 | 0.16 | 6.58 | 99.94 | 63 | 21 |
| *Tuape Shale* | | | | | | | | | | | | | | |
| T13 | 56.4 | 14.2 | 5.02 | 7.15 | 2.20 | 1.29 | 2.80 | 0.04 | 0.65 | 0.16 | 9.63 | 99.48 | 66 | 22 |
| T12 | 59.0 | 14.1 | 4.98 | 5.85 | 2.10 | 1.70 | 2.59 | 0.03 | 0.70 | 0.13 | 8.51 | 99.69 | 63 | 20 |
| T11 | 57.7 | 13.1 | 5.36 | 7.16 | 2.23 | 1.63 | 2.10 | 0.05 | 0.64 | 0.09 | 8.73 | 98.76 | 63 | 20 |
| T10 | 57.4 | 13.2 | 5.01 | 7.67 | 2.15 | 1.39 | 2.50 | 0.04 | 0.64 | 0.10 | 9.51 | 99.52 | 64 | 21 |
| T8 | 56.8 | 15.1 | 5.31 | 5.53 | 2.49 | 1.15 | 3.14 | 0.04 | 0.69 | 0.15 | 9.02 | 99.48 | 68 | 22 |
| T7 | 61.0 | 15.5 | 5.37 | 2.77 | 2.24 | 1.85 | 3.01 | 0.02 | 0.77 | 0.16 | 6.62 | 99.22 | 62 | 20 |
| T6 | 60.3 | 15.3 | 5.27 | 3.24 | 2.36 | 1.72 | 3.05 | 0.02 | 0.75 | 0.16 | 6.91 | 99.04 | 63 | 20 |
| T5 | 59.9 | 15.2 | 5.08 | 4.07 | 2.35 | 1.53 | 2.89 | 0.04 | 0.71 | 0.14 | 6.30 | 98.23 | 65 | 21 |
| T4 | 53.6 | 11.7 | 4.22 | 11.47 | 1.47 | 1.54 | 1.70 | 0.03 | 0.55 | 0.08 | 13.00 | 99.31 | 63 | 21 |
| *Cerro La Ceja* | | | | | | | | | | | | | | |
| T2 | 61.2 | 14.7 | 6.11 | 3.70 | 1.69 | 0.95 | 3.06 | 0.02 | 0.67 | 0.12 | 7.30 | 99.47 | 70 | 22 |
| T1 | 62.5 | 14.2 | 5.64 | 3.26 | 1.85 | 0.98 | 2.95 | 0.02 | 0.71 | 0.14 | 7.11 | 99.35 | 69 | 20 |

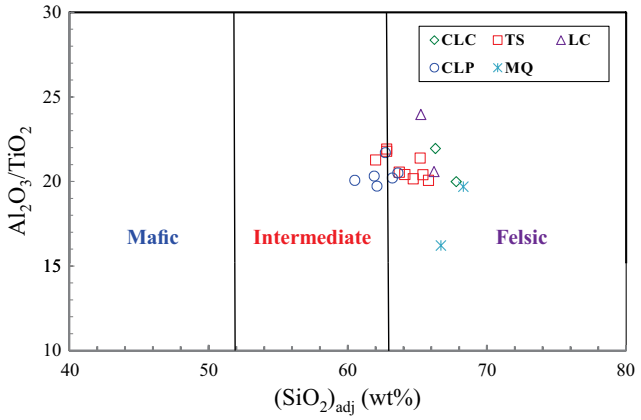


Figure 4. $Al_2O_3/TiO_2$ *vs.* $(SiO_2)_{adj}$ relationship for shales of the Mural Limestone. The fields based on $(SiO_2)_{adj}$ are from Le Bas et al. (1986).

not controlled by the clay minerals (Armstrong-Altrin *et al.*, 2014).

The concentrations of the redox-sensitive trace elements (Mo, U, and V) are given in Table 6. The CLC, LC and MQ members show low concentrations of Mo (0.62 – 0.69 ppm; 0.60 – 0.65 ppm; 0.67 – 0.68 ppm, respectively; Table 6) than TS and CLP members (0.65 – 3.09 ppm; 0.67 – 1.05 ppm; respectively). Under reducing conditions, the modern marine sediments are enriched with Mo where free $H_2S$ is present, with Black Sea reduced sediments containing 2 – 40 ppm and Saanich Inlet sediments 50 – 125 ppm (Crusius *et al.*, 1996), which are noticeably higher than the average Mo concentrations in normal shales (1 ppm) (Wedepohl, 1971, 1991) and in black shales (10 ppm) (Vine and Tourtelot, 1970). Uranium enrichment is found in the lower part of the TS Member and in the lower and middle parts of the CLP Member. However, CLC, LC and MQ members show low content of U (2.30 – 2.55 ppm; 2.27 – 2.42 ppm; 1.92 – 2.51 ppm; respectively). Low contents of U are found in sediments deposited in oxygenated conditions in marine environment (Somayajulu *et al.,* 1994), whereas sediments deposited from the oxygen minimum zone show high U contents (Barnes and Cochran, 1990; Klinkhammer and Palmer, 1991; Sarkar *et al.*, 1993; Somayajulu *et al.*, 1994; Nath *et al.*, 1997). Significant variations in vanadium content are observed among different members in the Tuape section.

**Rare earth elements**

The concentrations of rare earth elements are given in Table 7. The shale samples show large variations in ΣREE content among different members suggesting that the observed variations may be due to compositional variability. ΣREE contents positively correlate with $Al_2O_3$, suggesting that the ΣREE contents in these shales are controlled mainly by the clay minerals. In general, chondrite-normalized REE patterns (Figure 6) are stepped with considerable LREE enrichment, $((La/Sm)_{cn}$: 2.46 – 7.12, 4.81 ± 1.22, n = 21; cn refers to chondrite normalized values), flat HREE $((Gd/Yb)_{cn}$: 1.23 – 1.72, 1.35 ± 0.13, n = 21) with significant negative Eu anomalies (Eu/Eu*: 0.56 – 0.73, 0.65 ± 0.05, n = 21).

**Distribution of total organic carbon and total nitrogen concentrations**

A distinct variation in total organic carbon (TOC) content is found in the Tuape section, with values that range between 0.33% and 3.08%. The low variations in TOC content are observed in the Cerro La Ceja Member (0.85 – 0.91%; Table 6). The sudden increase in TOC content is noticed in the base of the Tuape Shale Member, and then gradually decrease in TOC value (1.18%) and the values then increase to 1.91%. Again, low TOC content is observed in the Los Coyotes Member. A gradual increase in TOC content (1.9%) is noticed in the base of the

Table 6. Concentration of trace elements (ppm) in shales from Tuape section of the Mural Limestone.

| | Sc | V | Cr | Co | Ni | Cu | Zn | Rb | Sr | Y | Zr | Nb | Mo | Ba | Hf | Pb | Th | U |
|---|---|---|---|---|---|---|---|---|---|---|---|---|---|---|---|---|---|---|
| *Mesa Quemeda* | | | | | | | | | | | | | | | | | | |
| T24 | 13.95 | 68.03 | 37.87 | 5.06 | 10.53 | 17.18 | 65.14 | 53.55 | 95.46 | 24.04 | 126.02 | 8.65 | 0.67 | 167.69 | 3.48 | 4.56 | 6.18 | 1.92 |
| T23 | 15.84 | 90.43 | 46.19 | 9.45 | 16.10 | 20.85 | 103.52 | 58.25 | 112.70 | 33.84 | 156.09 | 11.37 | 0.68 | 294.56 | 4.14 | 8.47 | 6.77 | 2.51 |
| *Cerro La Puerta* | | | | | | | | | | | | | | | | | | |
| T22 | 16.27 | 126.52 | 146.60 | 5.80 | 25.68 | 18.15 | 84.60 | 90.45 | 179.48 | 22.77 | 133.34 | 8.09 | 0.92 | 454.60 | 3.68 | 13.07 | 7.58 | 2.76 |
| T21 | 14.11 | 82.63 | 157.02 | 5.94 | 36.33 | 15.40 | 71.72 | 82.42 | 201.04 | 21.08 | 33.39 | 2.73 | 0.69 | 243.42 | 1.15 | 11.74 | 6.89 | 5.30 |
| T20 | 15.61 | 130.74 | 148.33 | 7.40 | 26.56 | 23.64 | 74.64 | 106.29 | 138.71 | 25.47 | 145.43 | 11.84 | 0.70 | 286.23 | 4.10 | 9.41 | 9.42 | 2.62 |
| T19 | 16.59 | 127.54 | 147.46 | 10.23 | 30.35 | 21.12 | 81.55 | 95.15 | 160.77 | 25.81 | 70.99 | 7.18 | 0.67 | 271.24 | 1.98 | 13.54 | 8.61 | 2.64 |
| T18 | 13.97 | 111.39 | 136.21 | 6.57 | 40.59 | 15.77 | 81.68 | 81.07 | 203.76 | 22.75 | 111.09 | 7.49 | 1.05 | 208.46 | 2.94 | 12.81 | 6.92 | 5.54 |
| T17 | 17.08 | 115.92 | 126.07 | 9.06 | 27.00 | 21.14 | 87.32 | 94.49 | 158.62 | 24.25 | 146.59 | 9.91 | 0.72 | 233.10 | 4.13 | 14.13 | 7.89 | 2.44 |
| *Los Coyotes* | | | | | | | | | | | | | | | | | | |
| T15 | 13.3 | 78.9 | 55.28 | 6.08 | 23.7 | 60.33 | 94.2 | 76.91 | 180.14 | 30.02 | 160.6 | 12.05 | 0.6 | 480.3 | 4.17 | 5.93 | 7.61 | 2.42 |
| T14 | 11.72 | 82.38 | 50.35 | 6.21 | 26.26 | 54.73 | 89.24 | 65.99 | 186.88 | 31.84 | 147.37 | 11.27 | 0.65 | 454.48 | 4.06 | 6.22 | 7.24 | 2.27 |
| *Tuape Shale* | | | | | | | | | | | | | | | | | | |
| T13 | 14.79 | 124.99 | 120.43 | 5.93 | 28.35 | 17.86 | 57.77 | 107.01 | 147.46 | 25.41 | 96.43 | 6.06 | 1.30 | 247.91 | 2.75 | 14.28 | 9.04 | 3.90 |
| T12 | 14.62 | 99.28 | 63.81 | 4.96 | 22.94 | 17.07 | 71.61 | 96.11 | 167.01 | 24.24 | 142.46 | 11.97 | 0.65 | 267.31 | 4.08 | 10.54 | 9.14 | 3.11 |
| T11 | 13.12 | 88.84 | 109.06 | 8.20 | 24.79 | 16.43 | 58.57 | 76.81 | 177.86 | 23.41 | 149.49 | 9.99 | 0.68 | 202.84 | 4.31 | 10.48 | 7.08 | 2.53 |
| T10 | 11.85 | 98.36 | 125.18 | 8.26 | 23.94 | 16.30 | 44.09 | 71.06 | 123.77 | 15.57 | 122.94 | 9.84 | 0.66 | 174.50 | 3.59 | 8.67 | 5.53 | 2.12 |
| T8 | 16.01 | 126.04 | 143.87 | 9.49 | 33.34 | 23.45 | 83.45 | 114.22 | 125.09 | 25.67 | 154.17 | 12.38 | 1.00 | 242.32 | 4.43 | 14.49 | 10.27 | 3.08 |
| T7 | 16.76 | 124.91 | 132.61 | 4.63 | 33.02 | 29.06 | 105.61 | 105.99 | 130.57 | 28.82 | 167.35 | 9.45 | 3.08 | 339.36 | 4.73 | 15.82 | 9.90 | 4.65 |
| T6 | 16.23 | 106.70 | 79.77 | 7.24 | 32.58 | 24.94 | 82.08 | 109.37 | 141.79 | 27.83 | 165.36 | 12.62 | 2.43 | 328.54 | 4.68 | 14.31 | 9.48 | 4.00 |
| T5 | 16.61 | 100.40 | 59.75 | 6.49 | 27.34 | 19.06 | 61.66 | 107.85 | 149.56 | 27.97 | 164.61 | 12.61 | 1.86 | 421.37 | 4.66 | 13.95 | 9.52 | 4.02 |
| T4 | 12.76 | 89.06 | 129.10 | 3.17 | 31.47 | 16.24 | 79.04 | 63.72 | 159.90 | 22.22 | 124.03 | 8.28 | 3.09 | 248.83 | 3.62 | 6.14 | 6.11 | 5.36 |
| *Cerro La Ceja* | | | | | | | | | | | | | | | | | | |
| T2 | 15.8 | 125.22 | 110.15 | 4.72 | 17.16 | 22.3 | 116.4 | 99.72 | 150.93 | 31.82 | 165.5 | 10.1 | 0.62 | 625 | 4.71 | 5.03 | 7.85 | 2.55 |
| T1 | 15.10 | 107.01 | 106.25 | 4.93 | 15.07 | 21.80 | 125.92 | 98.50 | 163.72 | 35.71 | 173.72 | 9.53 | 0.69 | 610.46 | 4.89 | 4.76 | 8.18 | 2.30 |

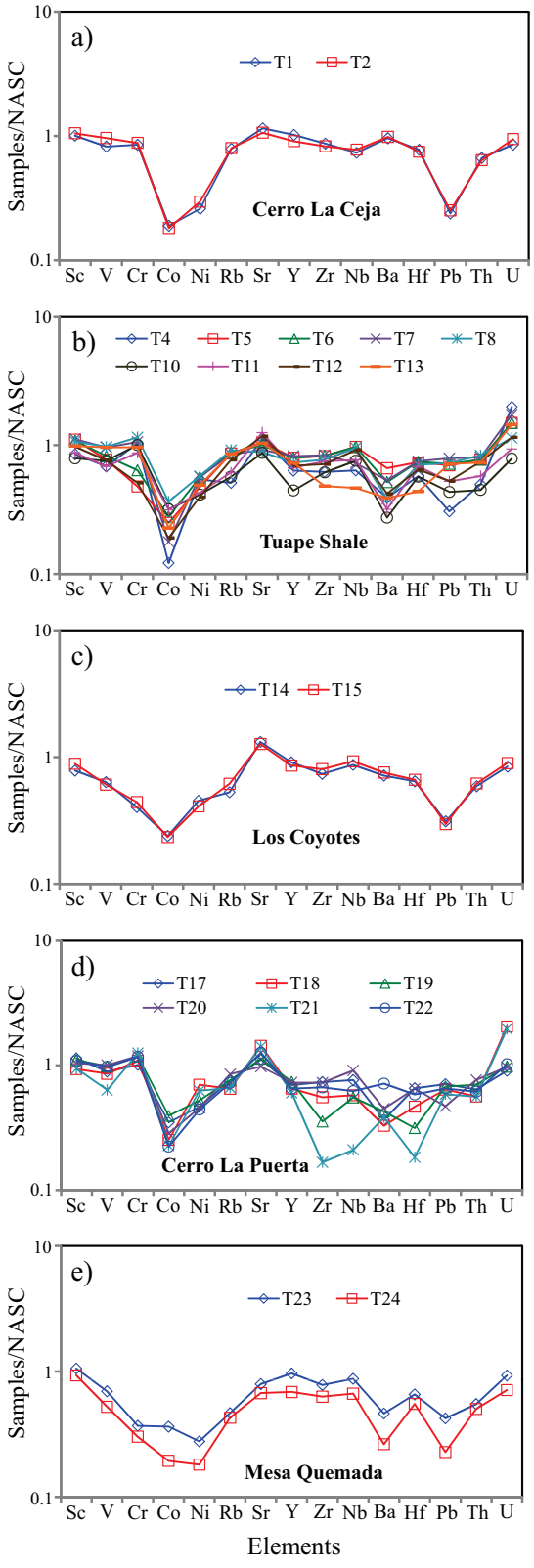


Figure 5. a) NASC-normalized trace elements diagram for shales of the Cerro La Ceja Member of the Mural Limestone; b) NASC-normalized trace elements spider diagram for shale samples of the Tuape Shale Member; c) NASC-normalized trace elements diagram for shales of the Los Coyotes Member; d) NASC-normalized spider diagram for shales of the Cerro La Puerta Member; e) NASC-normalized trace elements diagram for shale samples of the Mesa Quemada Member of the Mural Limestone.

Cerro La Puerta Member, and higher values of TOC are noticed in the middle part of this member (T18: 2.82%; T21: 2.42%). The Mesa Quemada Member has low TOC content (0.33 – 0.45%). The Al normalized distribution of total organic carbon (TOC) content of the Tuape section is shown in Figure 7. In this section, TOC concentration show significant positive shift in the lower part and slight increase in TOC values in the upper part of the TS Member. Likewise, two positive shifts are noticed in the CLP Member. Such positive shift in the TOC curve in the TS and CLP Members suggest that the depositional basin experienced fluctuations (oxic/anoxic) in the bottom water condition during the deposition of these shales. Total Nitrogen concentrations are higher in the TS and CLP members (0.04 – 0.08%; 0.04 – 0.06%; respectively) than CLC, LC and MQ members (0.04%; 0.04%: 0.03 – 0.04%; respectively).

## DISCUSSION

### Paleoclimate

In marine settings, the variations in bulk-rock mineralogy and clay fraction may record paleoenvironmental changes and/or a diagenetic overprint (Westermann *et al.*, 2013). As a consequence, before making any paleoenvironmental interpretation, it is essential to estimate the diagenetic changes in the clay mineral assemblages. Most authigenic clay-mineral formations (recrystallization and the formation of new minerals) occur during burial diagenesis. It has been demonstrated that burial diagenesis may result in the replacement of smectite by chlorite and illite in calcareous beds and marly interbeds, respectively, and an increase of the proportion of regularly mixed interstratified illite–smectite (I/S) with the burial depth (Chamley, 1989; Kübler and Jaboyedoff, 2000; Godet *et al.*, 2008). In the studied section, the regular mixed I/S is completely absent which indicates a significantly lower diagenetic overprint (Godet *et al.*, 2008). Furthermore, the diversity of the clay minerals and the presence of significant variations (>5%) in the mineralogical composition and the lack of any continuous vertical trend within the studied section suggest a relatively low impact on the primary environmental signal by burial diagenesis (Duchamp-Alphonse *et al.*, 2011). Hence, the trends observed in the clay-mineral assemblages in the present study can be used as paleoenvironmental proxies.

The clay mineralogical assemblages of the Tuape section have provided information on the environment of deposition and climatic conditions that prevailed during late Aptian-early Albian age. During the late Aptian, the source area experienced a warm climate with alternating wet and dry seasons, deciphered from the dominance of smectite and illite in the CLC Member. The rock-derived clay minerals (illite and chlorite) are dominant in the lower part of the TS, LC, upper part of the CLP and MQ members, suggesting the predominance of physical weathering over chemical weathering. Chlorite and illite are formed during the initial stages of weathering processes (Nesbitt and Young 1984, 1989; Weaver 1989; Fürsich *et al.*, 2005). The dominance of illite and chlorite in the sedimentary rocks indicate relatively fast erosion in the provenance area (Fürsich *et al.*, 2005). This pattern is typical of a paleoclimate change from warm and humid (seasonal) to arid or semi-arid (Ruffell and Batten, 1990; Madhavaraju *et al.*, 2002). In addition, the dominance of detrital chlorite could be an indication of an increasing continental landmass and reflecting more proximal depositional environments (Duarte, 1998).

The marked increase in kaolinite content (at the expense of mixed-layer clays) in the upper part of the TS and lower part of the CLP members suggest a change in the source area weathering from seasonal climates to chemical weathering. The occurrence of kaolinite indicates a source region which experienced intense weathering under possibly

tropical conditions (Biscaye, 1965) where increasing rainfall favoured ionic transfer and pedogenic development of kaolinite (Leung and Lai, 1965; Millot, 1970; Wang and Chen, 1988). We interpret the kaolinite as the end-product of rock degradation in the hinterland and *in situ* weathering profiles. The increasing concentration of kaolinite indicates the high water–rock ratio in the source area along with a humid-subtropical to tropical climate (Raucsik and Varga, 2008). Hence, the occurrence of both rock (illite and chlorite) and soil derived (kaolinite) clay minerals in the upper part of the TS and lower part of the CLP members suggests a warm and humid (seasonal) sub-tropical climate.

**Paleoweathering conditions**

The weathering intensity in the sedimentary rocks may be evaluated by using the relationship between alkali and alkaline earth elements (Nesbitt and Young, 1982). During weathering, the labile elements (Na, Ca, and Sr) are mainly leached from the weathering profile leaving behind the insoluble elements (Al, Ba, Rb) (Nesbitt *et al.*, 1980). These chemical changes are transferred to the sedimentary record (Nesbitt and Young 1982; Wronkiewicz and Condie, 1987), thus providing a useful tool for monitoring source area weathering conditions.

A chemical index widely used to determine the degree of source area weathering is the Chemical Index of Alteration, CIA (Nesbitt and Young, 1982). This index can be calculated using molecular proportions of the following oxides: CIA = $(Al_2O_3/Al_2O_3+CaO^*+Na_2O+K_2O)^*100$, where CaO* is the amount of CaO associated with the silicate fraction of the rock. CIA value gives the relative proportions of secondary aluminous clay minerals to primary silicate minerals like feldspars (Nesbitt and Young, 1982). Most of the shales show higher concentration of CaO (2.17 – 11.47%). Hence, the CaO values in these samples are not considered as CaO* and are not used for CIA calculation. For the present study, we have followed the method proposed by McLennan (1993) to calculate the CaO* in the sedimentary rocks. The CaO* content was calculated using the following methods: a) if the content of CaO was less or equal to the $Na_2O$ content, then we use the CaO value for further calculation, b) if the CaO content was higher than $Na_2O$, then $Na_2O$ value was considered as CaO* value (Bock *et al.*, 1998; Gallet *et al.*, 1998; Roddaz *et al.*, 2006; Újvarí *et al.*, 2008). The higher CIA values (76 to 100) in the sedimentary rocks suggest the intense chemical weathering in the source region (Fadipe *et al.*, 2011; Srivastava *et al.*, 2013; Újvarí *et al.*, 2013), whereas low values (50 or less) indicate the near absence of chemical weathering and also reflect cool and arid conditions (Fedo *et al.*, 1995).

The CIA values of the shales are given in Table 5. The shales from CLC, TS, LC, CLP and MQ members show small variations in CIA values (CIA: 69 – 70; 62 – 68; 63 – 64; 60 – 65; 59 – 65; respectively). CIA values of the present study are higher than the average NASC value of 57 (Gromet *et al.*, 1984) and slightly lower than the typical shale values (PAAS: 70 – 75; Taylor and McLennan, 1985). Therefore, the observed CIA values in the shales indicate the moderate chemical weathering intensity in the source rocks.

Another index to measure the chemical weathering of sediments and sedimentary rocks is Plagioclase Index of Alteration (PIA: Fedo *et al.*, 1995), which can be calculated as follows: PIA = $[(Al_2O_3 - K_2O)/(Al_2O_3+Na_2O+CaO^*-K_2O)] \times 100$ (molecular proportions). The PIA values of CLC, TS, LC, CLP and MQ members (PIA: 77 – 79; 66 - 76; 66 – 68; 63 – 72; 62 – 68; respectively) are consistent with CIA values which further support that these shales undergone moderate intensity of chemical weathering.

In addition, $Al_2O_3$ – $(CaO^*+Na_2O)$ – $K_2O$ (A-CN-K) diagram (molecular proportion; Fedo *et al.*, 1996; Figure 8) which categorizes the differentiation of compositional variations associated with chemical weathering and/or source rock composition (Deepthi *et al.*, 2012; Ghosh *et al.*, 2012). The A-CN-K diagram (Figure 8) displays a moderate loss of Ca, Na and K in the shale samples, as they tend to

Table 7. Concentration of rare earth elements (ppm) in shales from Tuape section of the Mural Limestone.

| | La | Ce | Pr | Nd | Sm | Eu | Gd | Tb | Dy | Ho | Er | Tm | Yb | Lu | ΣREE | Eu/Eu* |
|---|---|---|---|---|---|---|---|---|---|---|---|---|---|---|---|---|
| *Mesa Quemada* | | | | | | | | | | | | | | | | |
| T23 | 22.13 | 46.49 | 5.63 | 23.35 | 5.35 | 1.21 | 5.42 | 0.94 | 5.40 | 1.22 | 3.16 | 0.48 | 2.99 | 0.45 | 124.20 | 0.56 |
| T24 | 18.03 | 33.81 | 4.47 | 18.00 | 3.90 | 0.71 | 3.84 | 0.69 | 3.91 | 0.89 | 2.43 | 0.38 | 2.44 | 0.37 | 93.86 | 0.68 |
| Cerro La Puerta | | | | | | | | | | | | | | | | |
| T22 | 17.06 | 32.45 | 4.35 | 17.52 | 3.79 | 0.85 | 3.50 | 0.64 | 3.61 | 0.83 | 2.26 | 0.36 | 2.32 | 0.36 | 89.92 | 0.71 |
| T21 | 15.38 | 27.91 | 3.85 | 15.76 | 3.49 | 0.83 | 3.24 | 0.60 | 3.39 | 0.76 | 2.07 | 0.33 | 2.10 | 0.32 | 80.05 | 0.76 |
| T20 | 25.00 | 50.67 | 5.97 | 23.39 | 4.87 | 0.95 | 4.57 | 0.78 | 4.33 | 0.96 | 2.59 | 0.40 | 2.57 | 0.39 | 127.44 | 0.61 |
| T19 | 22.11 | 45.85 | 5.38 | 21.47 | 4.58 | 0.93 | 4.29 | 0.76 | 4.24 | 0.96 | 2.58 | 0.40 | 2.58 | 0.39 | 116.52 | 0.64 |
| T18 | 16.07 | 30.16 | 4.19 | 17.07 | 3.73 | 0.85 | 3.41 | 0.62 | 3.53 | 0.80 | 2.17 | 0.34 | 2.19 | 0.33 | 85.46 | 0.73 |
| T17 | 19.06 | 38.01 | 4.72 | 19.15 | 4.20 | 0.88 | 3.96 | 0.71 | 4.06 | 0.93 | 2.52 | 0.40 | 2.59 | 0.39 | 101.58 | 0.66 |
| *Los Coyotes* | | | | | | | | | | | | | | | | |
| T15 | 27.34 | 52.38 | 6.70 | 27.71 | 5.80 | 1.30 | 5.75 | 1.00 | 5.35 | 1.20 | 3.15 | 0.48 | 2.83 | 0.46 | 141.45 | 0.69 |
| T14 | 25.12 | 48.18 | 6.53 | 26.68 | 5.86 | 1.26 | 5.68 | 0.94 | 5.12 | 1.13 | 2.91 | 0.43 | 2.67 | 0.40 | 132.89 | 0.67 |
| *Tuape Shale* | | | | | | | | | | | | | | | | |
| T13 | 23.37 | 46.58 | 5.66 | 22.52 | 4.67 | 0.95 | 4.25 | 0.74 | 4.10 | 0.92 | 2.48 | 0.39 | 2.48 | 0.38 | 119.48 | 0.65 |
| T12 | 23.98 | 46.02 | 5.69 | 22.32 | 4.55 | 0.90 | 4.20 | 0.71 | 3.91 | 0.88 | 2.35 | 0.37 | 2.40 | 0.36 | 118.66 | 0.63 |
| T11 | 19.29 | 38.57 | 4.75 | 19.01 | 3.99 | 0.78 | 3.66 | 0.66 | 3.79 | 0.87 | 2.35 | 0.37 | 2.41 | 0.37 | 100.88 | 0.62 |
| T10 | 14.27 | 26.53 | 3.35 | 13.28 | 2.79 | 0.53 | 2.43 | 0.45 | 2.56 | 0.57 | 1.60 | 0.26 | 1.65 | 0.25 | 70.51 | 0.62 |
| T8 | 26.09 | 52.00 | 5.89 | 22.47 | 4.75 | 0.83 | 4.39 | 0.77 | 4.38 | 0.99 | 2.64 | 0.41 | 2.66 | 0.40 | 128.69 | 0.56 |
| T7 | 26.25 | 51.35 | 6.26 | 24.66 | 5.17 | 1.00 | 4.72 | 0.82 | 4.69 | 1.06 | 2.90 | 0.45 | 2.91 | 0.45 | 132.71 | 0.62 |
| T6 | 25.59 | 51.35 | 6.19 | 24.22 | 5.08 | 0.99 | 4.59 | 0.81 | 4.57 | 1.03 | 2.78 | 0.43 | 2.81 | 0.43 | 130.86 | 0.63 |
| T5 | 23.70 | 48.16 | 5.91 | 23.43 | 4.97 | 1.01 | 4.72 | 0.81 | 4.61 | 1.04 | 2.82 | 0.44 | 2.86 | 0.43 | 124.88 | 0.64 |
| T4 | 16.61 | 29.28 | 4.38 | 17.83 | 3.86 | 0.88 | 3.59 | 0.65 | 3.65 | 0.81 | 2.17 | 0.34 | 2.18 | 0.33 | 86.57 | 0.72 |
| *Cerro La Ceja* | | | | | | | | | | | | | | | | |
| T1 | 26.52 | 51.75 | 6.59 | 26.95 | 5.87 | 1.17 | 5.65 | 0.99 | 5.72 | 1.32 | 3.53 | 0.54 | 3.45 | 0.53 | 140.59 | 0.61 |
| T2 | 25.10 | 48.54 | 5.81 | 24.76 | 5.50 | 1.10 | 5.48 | 0.92 | 5.57 | 1.25 | 3.50 | 0.50 | 3.41 | 0.50 | 131.94 | 0.62 |

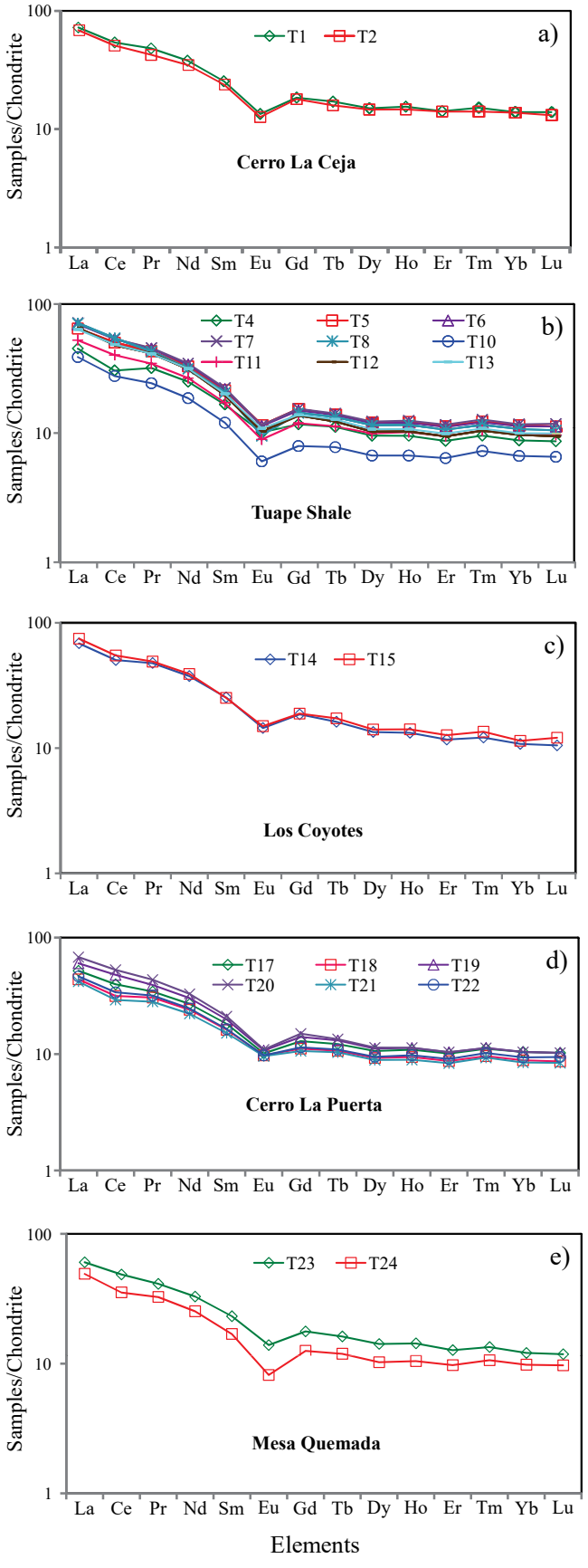


plot between feldspar join line and A apex. Therefore, the positions of samples in the A-CN-K diagram, as well as their CIA and PIA values, indicate that these sediments were generated from a rock source affected by moderate intensity of chemical weathering. The degree of weathering in the source area was higher than that of NASC and this is shown by the moderate depletion not only in the elements selectively leached from weathering profiles, such as Na, Ca and Sr (Nesbitt *et al.*, 1980; Wronkiewicz and Condie, 1987), but also in the relatively large cations, such as K, Rb and Ba. These elements are mainly fixed on clays such as illite. In particular, the CIA values of the samples collected from the weathering profile are more or less parallel to the A-CN line of A-CN-K plot (Nesbitt and Young, 1984; Fedo *et al.*, 1995).

**Provenance**

Trace element compositions could potentially be a source of information to determine provenance. The high field strength elements Zr, Hf, Y and Nb are relatively immobile in the sedimentary environment (as do Al and Ti), thus they reflect provenance composition (Taylor and McLennan, 1985). $Al_2O_3/TiO_2$ ratios in clastic sedimentary rocks are considered as a powerful tool to understand the types of source rocks (Garcia *et al.*, 1994; Andersson *et al.*, 2004), since the ratio < 14 in sediments is indicative of mafic source rocks, whereas ratios ranging from 19 to 28 reveal felsic source rocks. $Al_2O_3/TiO_2$ ratios in the shales of the Mural Formation, which range from 16 to 22 (Table 5), suggest that these sediments have been derived predominantly from felsic source rocks.

The REE patterns and size of Eu anomaly in the sedimentary rocks can be considered as an important clue to unravel the source rock signatures (Taylor and McLennan, 1985; Madhavaraju and Lee, 2010; Fu *et al.*, 2010; Armstrong-Altrin *et al.*, 2013). In general, the felsic rocks mainly exhibit higher LREE/HREE ratios and negative Eu anomaly, while mafic rocks show lower LREE/HREE ratios with little or no Eu anomaly (Cullers *et al.*, 1987; Cullers, 1994). All shale samples analyzed in this study have fractionated chondrite-normalized REE patterns, negative Eu anomalies (Eu/Eu*: 0.56 – 0.76; Table 7), LREE enriched, and flat HREE patterns (LREE/HREE: 5.14 – 6.75). Such REE patterns suggest that the original source area was felsic in composition.

**Paleo-redox conditions**

*Significance of higher TOC/TN values in the black shale sequences*

The marine organic matter, usually has TOC/TN values between 5 and 8 (Emerson and Hedges, 1988; Meyers, 1994); however, higher TOC/TN values (between 20 and 40) are common in Albian-Cenomanian black shales deposited around the world (Rau *et al.*, 1987; Meyers, 1989; Dumitrescu and Brassell, 2006). The higher TOC/TN values are also found in modern sediments deposited under areas of high productivity. Verardo and MacIntyre (1994) mentioned that the higher values indicate more rapid loss of nitrogen than carbon during sinking of marine organic matter from the photic zone. In the present study, most of the black shales of TS and CLP members show TOC/TN values between 20 and 40 (except one sample that show lower value of

Figure 6. a. Chondrite normalized rare earth elements patterns for shales of the Cerro La Ceja Member; b. Chondrite normalized rare earth elements patterns for shales of the Tuape Shale Member; c. Chondrite normalized rare earth elements patterns for shales of the Los Coyotes Member; d. Chondrite normalized rare earth elements patterns for shales of the Cerro La Puerta Member; e. Chondrite normalized rare earth elements patterns for shale samples of the Mesa Quemada Member of the Mural Limestone.

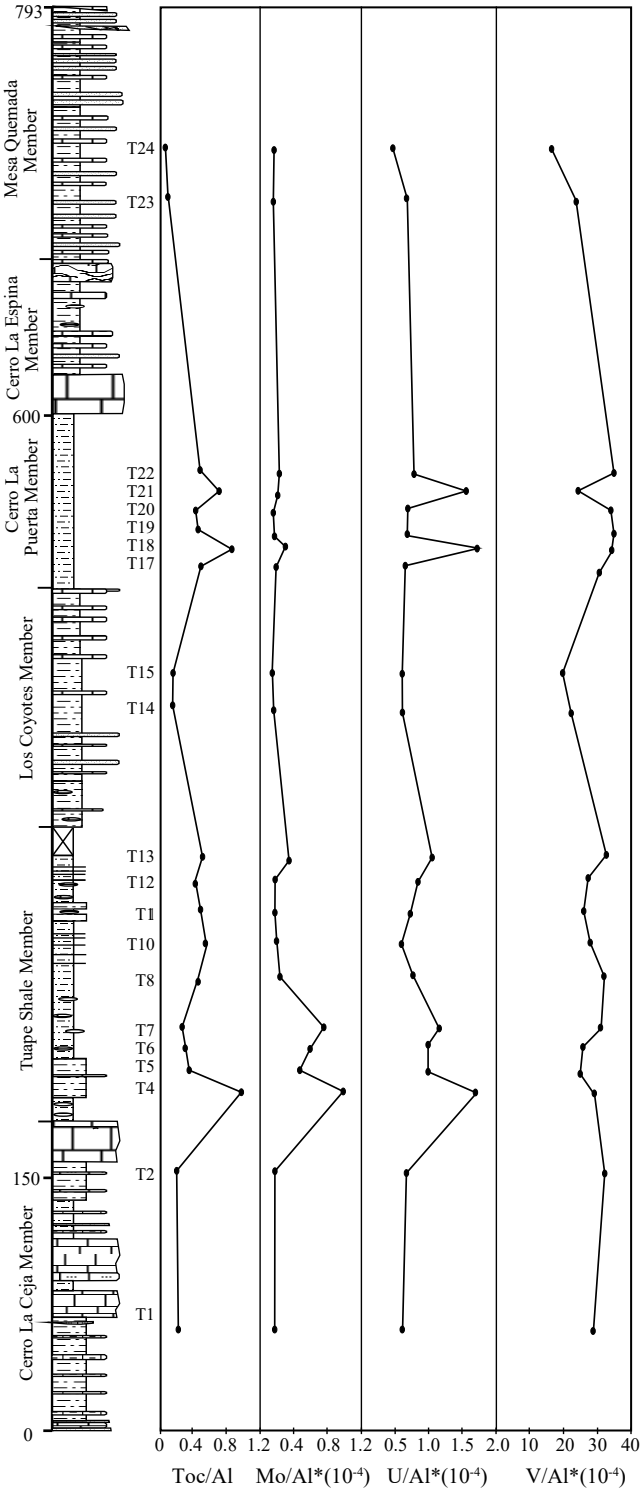


Figure 7. Al normalized vertical distribution patterns for TOC and redox-sensitive trace elements (Mo, U and V) for shales of the Mural Limestone.

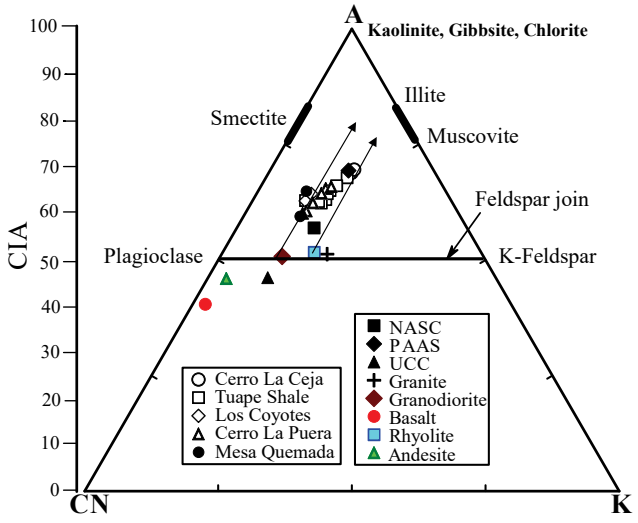


Figure 8. A-CN-K diagram showing the weathering trend of the Mural Limestone (after Nesbitt and Young, 1982). A: $Al_2O_3$; CN: $CaO^* + Na_2O$; K: $K_2O$ (molecular proportions).

17). According to Van Mooy *et al.* (2002), the degradation of marine organic matter differs significantly in suboxic and oxic conditions. Oxygen-deficient zones commonly are well-developed under areas of high productivity because the large fluxes of sinking organic matter deplete dissolved oxygen. Hence, the observed high TOC/TN values in TS and CLP members suggest that they were deposited in association with oxygen depletion that had developed under conditions of high productivity. Few black shale samples of TS and CLP members (T4, T18, T22; Table 6) show extremely higher TOC/TN values indicating that these samples contain important proportions of land–plant organic matter. The TOC/TN value of 81 in the carbonized wood in the lower Cenomanian sample clearly identifies the organic matter of this sample as land–plant woody tissue (Meyers, 1994). In addition, such higher TOC/TN values (between 40 and 60) are also observed in the lower Cenomanian and Albian samples from Ocean Drilling Program (ODP) Leg 2017 drill-sites on Demerara Rise sequences, offshore of northeastern South America (Meyers *et al.*, 2006).

*Multi-proxy trace element patterns*

The organic-rich black shales of Phanerozoic age are enriched in Mo, U and V (Brumsack and Gieskes, 1983; Brumsack, 2006; Coveney *et al.*, 1991; Sun and Puttmann, 1997; Nijenhuis *et al.*, 1999; Warning and Brumsack, 2000; Yarincik *et al.*, 2000; Mangini *et al.*, 2001; Tribovillard *et al.*, 2004; Wilde *et al.*, 2004). Uranium and vanadium enrichments are mainly associated with anoxic to euxinic bottom-water conditions during the time of deposition (Mangini *et al.*, 2001). The adsorption of Mo onto humic substances is a possible mechanism to transfer this element from the water column into the sediment, and under euxinic conditions, by rapid uptake by authigenic/syngenetic sulfides (Algeo and Maynard, 2004).

The multi-elements proxies are more suitable for the analysis of the paleo-redox conditions rather than a single elemental proxy (Tribovillard *et al.*, 2006). In this connection, the trace elements such as Mo, U and V are utilized because these elements are least vulnerable to primary and secondary complications (Tribovillard *et al.*, 2006). The Al normalized distribution of Mo, U and V contents of the Tuape section is shown in Figure 7. In this section, Mo and U concentrations show positive shifts in the lower part of the TS Member. However, no such positive shifts are observed in the vanadium curve. Likewise, Mo, U and V curves show small positive shift in the upper part of the TS Member (Figure 8). For the CLP Member, Mo curve shows a small positive shift, whereas U curve shows two positive shifts in the lower part of this member. In this member, two positive shifts of U are remarkable. However, CLP Member shows no such positive shift in the V curve (Figure 7). The observed positive shift in the Mo, U and

V curves in the TS and CLP members suggest that the depositional basin experienced the suboxic/anoxic bottom water condition during the deposition of these shales.

U/Th and Ni/Co ratios of marine sediments are considered as a reliable proxies to deduce the bottom water oxygenation conditions of the depositional environment (Dypvik, 1984; Wignall and Myers, 1988; Madhavaraju and Ramasamy, 1999; Hatch and Leventhal, 1992; Jones and Manning, 1994; Rimmer, 2004; Nagarajan *et al.*, 2007a; Madhavaraju and Lee, 2009; Madhavaraju and González-León, 2012; Madhavaraju *et al.*, 2016). A low U/Th ratio (< 0.75) suggests oxic conditions, whereas high U/Th ratio (> 1.25) indicates anoxic conditions (Jones and Manning, 1994). The CLC, LC and MQ members show lower U/Th ratios (0.28 – 0.32; 0.31 – 0.32; 0.31 – 0.37, respectively; Figure 9) than TS and CLP members (0.30 – 0.88; 0.28 – 0.80, respectively; Figure 9). The lower part of the TS Member and the lower and middle parts of the CLP Member have higher values of the U/Th ratio (> 0.75). The observed variations in U/Th ratio suggest that the fluctuation in U/Th ratio are mainly due to variations in oxygenation level from oxic to suboxic conditions.

The Ni/Co ratio has been considered to be a redox indicator by several researchers (Dypvik, 1984; Dill, 1986; Jones and Manning, 1994). Ni/Co ratios below 5 suggest oxic environments, whereas ratios above 5 suggest suboxic and anoxic environments (Jones and Manning, 1994). Significant variations in nickel and cobalt contents are observed in the shale samples of the different members of the Mural Limestone (Table 6). The CLC, LC and MQ members show low Ni/Co values (3.06 – 3.64; 3.90 – 4.23; 1.60 – 2.08, respectively; Figure 9) whereas the TS and CLP members show low to high Ni/Co content (2.90 – 9.94; 2.97 – 6.17, respectively; Figure 9). The lower part of the TS Member (7.13 to 9.94) and the lower and middle parts of the CLP Member (6.12 – 6.17) show higher values of the Ni/Co ratio (> 5). It suggests that the fluctuation in Ni/Co ratio was controlled mainly by the oxygenation level in the depositional basin (oxic to anoxic conditions).

The shale samples show large variations in Mo, U and V contents and Ni/Co and U/Th ratios. The combined use of trace elements and their ratios may allow to distinguish the various depositional environments, *i.e.* oxic-anoxic-euxinic. The CLC, LC and MQ members show relatively low contents of TOC, TN, Mo, U and V and low Ni/Co and U/Th ratios, suggesting that these shales were deposited under oxic conditions. The relatively low to moderate contents of TOC, TN, Mo, U and V, and elemental ratios of the TS and CLP members suggest that the depositional basin experienced large fluctuation in oxygen level during the deposition of these members, which resulted in the varying depositional conditions (oxic - suboxic - anoxic).

## CONCLUSIONS

The clay mineralogical assemblages (illite-chlorite-kaolinite-smectite) of the Tuape section have provided information on the climatic conditions and environment of deposition that prevailed during late Aptian-early Albian age. Illite and smectite are the dominant clay minerals identified in the CLC Member suggesting that the source area experienced a warm climate with alternating wet and dry seasons during the late Aptian. The lower part of the TS, LC, upper part of the CLP and MQ members are rich in rock-derived illite and chlorite, suggesting the predominance of physical weathering over chemical weathering, and the source region experienced arid or semi-arid climatic conditions. The upper part of the TS and lower part of the CLP members show both rock (illite and chlorite) and soil derived (kaolinite) clay minerals that suggests a warm and humid (seasonal) sub-tropical climate.

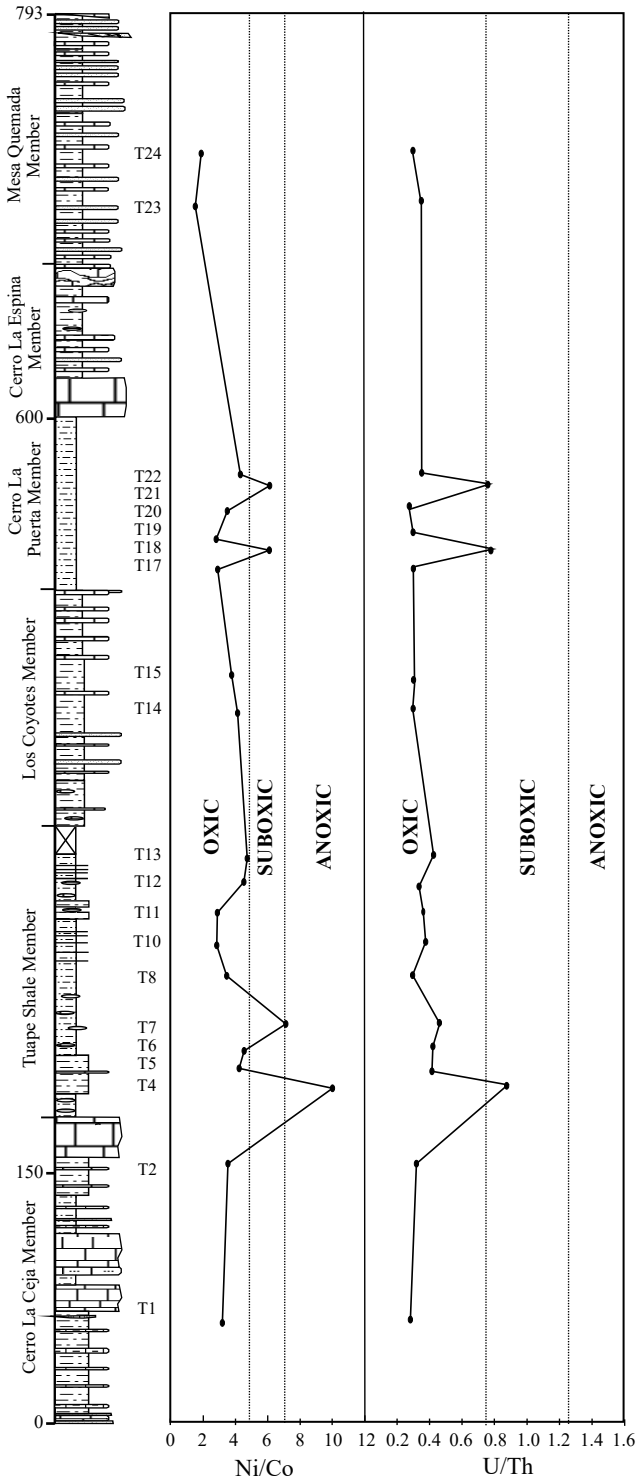


Figure 9. Ni/Co and U/Th variations in the shale samples from the Tuape section of the Mural Limestone.

The chondrite-normalized REE patterns of the shales are characterized by enriched LREE, relatively flat HREE and significant negative Eu anomalies. The shale samples from CLC, TS, LC, CLP and MQ members show small variations in CIA values: 69 – 70; 62 – 68; 63 – 64; 60 – 65; 59 – 65, respectively, which are higher than the average NASC value of 57 (Gromet *et al.*, 1984) and slightly lower than the typical shale PAAS values : 70 – 75 (Taylor and McLennan, 1985). The CIA and PIA

values and positions of samples in the A-CN-K diagram indicate that these shale samples were generated from a source rocks of the upper continental crust affected by moderate intensity of chemical weathering. The shale samples show large variations in Mo, U and V contents and Ni/Co and U/Th ratios. The low contents of TOC, TN, Mo, U and V and low Ni/Co and U/Th ratios in the CLC, LC and MQ members suggest that these shales have been deposited under oxic conditions. On the other hand, the TS and CLP members show relatively low to moderate contents of redox sensitive elements and their ratios suggest that the depositional basin experienced large oscillations in oxygen level during the deposition of these shales that resulted in the unstable depositional conditions (oxic - suboxic - anoxic).

## ACKNOWLEDGEMENTS

We acknowledge the support rendered by Universidad Nacional Autónoma de México through PAPIIT Project No.IN121506-3. We would like to thank Mr. Rufino Lozano-Santa Cruz and P. Girón García for their help in XRF analysis. We would like to thank Mr. Pablo Peñaflor for powdering of samples for geochemical studies. We also thank Dra. L. Mora Palomino, Instituto de Geología, Universidad Nacional Autónoma de México, México for her help in TOC and TN analysis. Finally, we also like to thank Departamento de Geología of the Universidad de Sonora for the support provided to Erick Ramírez-Montoya for his thesis work.

## REFERENCES

Ahlberg, A., Olsson, I., Šimkevičius, P., 2003, Triassic–Jurassic weathering and clay mineral dispersal in basement areas and sedimentary basins of southern Sweden: Sedimentary Geology, 161, 15-29.

Algeo, T.J., Maynard, J.B., 2004, Trace-element behavior and redox facies in core shales of Upper Pennsylvanian Kansas-type cyclothems: Chemical Geology, 206, 289-318.

Andersson, P.O.D., Worden, R.H., Hodgson, D.M., Flint, S., 2004, Provenance evolution and chemostratigraphy of a Palaeozoic submarine fan-complex: Tanqua Karoo Basin, South Africa: Marine and Petroleum Geology, 21, 555-577.

Armstrong-Altrin, J.S., 2009, Provenance of sands from Cazones, Acapulco, and Bahía Kino beaches, México: Revista Mexicana de Ciencias Geológicas, 26, 764-782.

Armstrong-Altrin, J.S., Nagarajan, R., Madhavaraju, J., Rosalez-Hoz, L., Lee, Y.I., Balaram, V., Cruz-Martínez, A., Avila-Ramírez, G., 2013, Geochemistry of the Jurassic and Upper Cretaceous shales from the Molango Region, Hidalgo, eastern Mexico: Implications for source-area weathering, provenance, and tectonic setting: Comptes Rendus Geoscience, 345, 185-202.

Armstrong-Altrin, J.S., Nagarajan, R., Lee, Y.I., Kasper-Zubillaga, Cordoba-Saldaña, L.P., 2014, Geochemistry of sands along the San Nicolas and San Carlos beaches, Gulf of California, Mexico: implications for provenance, and tectonic setting: Turkish Journal of Earth Sciences, 23, 533-558.

Armstrong-Altrin, J.S., Machain-Castillo, M.L., Rosales-Hoz, L., Carranza-Edwards, A., Sanchez-Cabeza, J.A., Ruíz-Fernández, A.C., 2015, Geochemistry of deep sea sediments from the south-western Gulf of Mexico, Mexico: implication for depositional environment: Continental Shelf Research, 95, 15-26.

Baioumy, H.M., Ismael, I.S., 2010, Factors controlling the compositional variations among the marine and non-marine black shales from Egypt: International Journal of Coal Geology, 83, 35-45.

Barnes, U.C., Cochran, J.R., 1990, Uranium removal in oceanic sediments and the oceanic U balance: Earth and Planetary Science Letters, 97, 94-101.

Bilodeau, W.L., Linberg, F.A., 1983, Early Cretaceous tectonics and sedimentation in southern Arizona, southwestern New Mexico, and northern Sonora, Mexico, *in* Reynolds, M.W., Dolly, E.D. (eds.), Mesozoic paleogeography of West-Central United States: Society of Economic Paleontologists and Mineralogists, Rocky Mountain Section, Rocky Mountain Paleogeography Symposium, 2, 173-188.

Bilodeau, W.L., Kluth, C.F., Vedder, L.K., 1987, Regional stratigraphic, sedimentologic, and tectonic relationships of the Glance Conglomerate in southeastern Arizona, *in* Dickinson, W.R., Klute, M.F. (eds.), Mesozoic rocks of southern Arizona adjacent areas: Arizona Geological Society Digest, 18, 229-256.

Biscaye, B.E., 1965, Mineralogy and sedimentation of recent deep sea clay in the Atlantic Ocean and adjacent seas and oceans: Geological Society of America Bulletin, 76, 803-832.

Bock, B., McLennan, S.M., Hanson, G.N., 1998, Geochemistry and provenance of the Middle Ordovician Austin Glen Member (Normanskill Formation) and the Taconian Orogeny in New England: Journal of Sedimentary Research, 45, 635-655.

Brindley, G.W., Brown, G., 1980, Crystal Structures of Clay Minerals and their X-Ray Identification: London, Mineralogical Society, 495 p.

Brumsack, H.J., 2006, The trace metal content of recent organic carbon-rich sediments: implications for Cretaceous black shale formation: Palaeogeography Palaeoclimatology Palaeoecology, 232, 344-361.

Brumsack, H.J., Gieskes, J.M., 1983, Interstitial water trace-element chemistry of laminated sediments of the Gulf of California (Mexico): Marine Chemistry, 14, 89-106.

Calvert, S.E., Pedersen, T.F., 1993, Geochemistry of recent oxic and anoxic sediments: implications for the geological record: Marine Geology, 113, 67-88.

Canet, C., Alfonso, P., Melgarejo, J.C., Belyatsky, B.V., 2004, Geochemical evidences of sedimentary-exhalative origin of the shale-hosted PGE-Ag-Au-Zn-Cu occurrences of the Prades Mountains (Catalonia, Spain): Trace-element abundances and Sm-Nd isotopes: Journal of Geochemical Exploration, 82, 17-33.

Cantú-Chapa, A., 1976, Nuevas localidades del Kimeridgiano y Titoniano en Chihuahua (Norte de México): Revista del Instituto Mexicano del Petróleo, 7, 38-45.

Chamley, H., 1989, Clay Sedimentology: Springer Verlag, Berlin Heidelberg New York, 623 pp.

Coveney, J.R.M., Lynn Watney, W., Maples, C.G., 1991, Contrasting depositional models for Pennsylvanian black shale discerned from molybdenum abundances: Geology, 19,147-150.

Cox, R., Lowe, D.R., Cullers, R.L., 1995, The influence of sediment recycling and basement composition on evolution of mudrock chemistry in the southwestern United States: Geochimica et Cosmochimica Acta, 59, 2919-2940.

Crusius, J., Calvert, S., Pedersen, T., Sage, D., 1996, Rhenium and molybdenum enrichments in sediments as indicators of oxic, suboxic and sulfidic conditions of deposition: Earth and Planetary Science Letters, 145, 65-78.

Cullers, R.L., 1994, The controls on the major and trace element variation of shales, siltstones, and sandstones of Pennsylvanian-Permian age from uplifted continental blocks in Colorado to platform sediment in Kansas, USA: Geochimica et Cosmochimica Acta, 58, 4955-4972.

Cullers, R.L., 1995, The controls on the major and trace element evolution of shales, siltstones and sandstones of Ordovician to Tertiary age in the Wet Mountain region, Colorado, USA: Chemical Geology, 123, 107-131.

Cullers, R.L., 2000,The geochemistry of shales, siltstones and sandstones of Pennsylvanian – Permian age, Colorado, USA: implications for provenance and metamorphic studies: Lithos, 51, 181-203.

Cullers, R.L., 2002, Implications of elemental concentrations for provenance, redox conditions, and metamorphic studies of shales and limestones near Pueblo, CO, USA: Chemical Geology, 191, 305-327.

Cullers, R.L., Barrett, T., Carlson, R., Robinson, B., 1987, Rare earth element and mineralogic changes in Holocene soil and stream sediment: a case study in the Wet Mountains, Colorado, USA: Chemical Geology, 63, 275-297.

DaPeng, L., YueLong, C., Zhong, W., Yu, L., Jian, Z., 2012, Paleozoic sedimentary record of the Xing-Meng Orogenic Belt, Inner Mongolia: implications for the provenances and tectonic evolution of the Central Asian Orogenic Belt: Chinese Science Bulletin, 57, 776-785.

Deconinck, J.F., Amedro, F., Baudin, F., Godet, A., Pellenard, P., Robaszynski, F., Zimmerlin, I., 2005, Late Cretaceous palaeoenvironments expressed by the clay mineralogy of Cenomanian - Campanian chalks from the east

of the Paris Basin: Cretaceous Research, 26, 171-179.
Deepthi, K., Natesan, U., Muthulakshmi, A.L., Ferrer, V.A., Venugopalan, V.P., Narasimhan, S.V., 2012, Geochemical characteristics and depositional environment of Kalpakkam, Southeast coast of India: Environmental Earth Science, http://dx.doi.org/10.1007/s12665-012-2065-5.
Dera, G., Pellenard, P., Neige, P., Deconinck, J.F., Pucéat, E., Dommergues, J.L., 2009, Distribution of clay minerals in Early Jurassic Peritethyan seas: palaeoclimatic significance inferred from multiproxy comparisons: Palaeogeography Palaeoclimatology Palaeoecology, 271, 39-51.
Dickinson, W.R., Klute, M.A., Swift, P.A., 1989, Cretaceous strata of southern Arizona, *in* Jenney, J.P., Reynols, S.J. (eds.), Geologic Evolution of Arizona: Arizona Geological Society Digest, 17, 447-462.
Dill, H., 1986, Metallogenesis of early Paleozoic graptolite shales from the Graefenthal Horst (northern Bavaria-Federal Republic of Germany): Economic Geology, 81, 889-903.
Duarte, L.V., 1998, Clay minerals and geochemical evolution in the Toarcian–Lower Aalenian of the Lusitanian Basin (Portugal): Cuadernos de Geología Ibérica, 24, 69-98.
Duchamp-Alphonse, S., Fiet, N., Adatte, T., Pagel, M., 2011, Climate and sea-level variations long the northwestern Tethyan margin during the Valanginian C-isotope excursion: mineralogical evidence from the Vocontian Basin (SE France): Palaeogeography Palaeoclimatology Palaeoecology, 302, 243-254.
Dumitrescu, M., Brassell, S.C., 2006, Compositional and isotopic characteristics of organic matter for the early Aptian Oceanic Anoxic Events at Shatsky Rise, ODP leg 198: Palaeogeography Palaeoclimatology Palaeoecology 235, 168-191.
Dypvik, H., 1984, Geochemical compositions and depositional conditions of Upper Jurassic and Lower Cretaceous Yorkshire clays, England: Geological Magazine, 121, 489-504.
Eggins, S.M., Woodhead, J.D., Kinsley, L.P.J., Mortimer, G.E., Sylvester, P., McCulloch, M.T., Hergt, J.M., Handler, M.R., 1997, A simple method for the precise determination of >=40 trace elements in geological samples by ICPMS using enriched isotope internal standardization: Chemical Geology, 134, 311-326.
Emerson, S., Hedges, J.I., 1988, Processes controlling the organic carbon content of open ocean sediments: Paleoceanography, 3, 621-634.
Etemad-Saeed, N., Hosseini-Barzi, M., Armstrong-Altrin, J.S., 2011, Petrography and geochemistry of clastic sedimentary rocks as evidence for provenance of the Lower Cambrian Lalun Formation, Posht-ebadam block, Central Iran: Journal of African Earth Sciences, 61, 142-159.
Fadipe, O.A., Carey, P.F., Akinlua, A., Adekola, S.A., 2011, Provenance, diagenesis and reservoir quality of the Lower Cretaceous sandstone of the Orange Basin, South Africa: South African Journal of Geology, 114, 433-448.
Fatima, S., Khan, M.S., 2012, Petrographic and geochemical characteristics of Mesoproterozoic Kumbalgarh clastic rocks, NW Indian shield: implications for provenance, tectonic setting, and crustal evolution: International Geology Review, 54, 1113-1144.
Fedo, C.M., Nesbitt, H.W., Young, G.M., 1995, Unraveling the effects of potassium metasomatism in sedimentary rocks and paleosoils, with implications for paleoweathering conditions and provenance: Geology, 23, 921-924.
Fedo, C.M., Eriksson, K., Krogstad, E.J., 1996, Geochemistry of shales from the Archean (3.0 Ga) Buhwa Greenstone Belt, Zimbabwe: Implications for provenance and source-area weathering: Geochimica et Cosmochimica Acta, 60, 1751-1763.
Fu, X., Wang, J., Zeng, Y., Tan, F., Feng, X., 2010, REE geochemistry of marine oil shale from the Changshe Mountain area, northern Tibet, China: International Journal of Coal Geology, 81, 191-199.
Fürsich, F.T., Singh, I.B., Joachimski, M., Krumm, S., Schlirf, M., Schlirf, S., 2005, Palaeoclimate reconstructions of the Middle Jurassic of Kachchh (western India): an integrated approach based on palaeoecological, oxygen isotopic, and clay mineralogical data: Palaeogeography Palaeoclimatology Palaeoecology, 217, 289-309.
Gallet, S., Jahn, B., Lanoë, B.V.V., Dia, A., Rossello, E., 1998, Loess geochemistry and its implications for particle origin and composition of the upper continental crust: Earth and Planetary Science Letters, 156, 157-172.
Garcia, D., Fonteilles, M., Moutte, J., 1994, Sedimentary fractionations between Al, Ti, and Zr and the genesis of strongly peraluminous granites: The Journal of Geology, 102, 411-422.
Ghosh, S., Sarkar, S., Ghosh, P., 2012, Petrography and major element geochemistry of the Permo-Triassic sandstones, central India: implications for provenance in an intracratonic pull-apart basin: Journal of Asian Earth Science, 43, 207-240.
Godet, A., Bodin, S., Adatte, T., Föllmi, K., 2008, Platform-induced clay-mineral fractionation along northern Tethyan basin-platform transect: implications for the interpretation of Early Cretaceous climate change (Late Hauterivian-Early Aptian): Cretaceous Research, 29, 830-847.
González-León, C.M., Scott, R.W., Loser, H., Lawton, T.F., Robert, E., Valencia, V.A., 2008, Upper Aptian-Lower Albian Mural Formation: stratigraphy, biostratigraphy and depositional cycles on the Sonoran shelf, northern Mexico: Cretaceous Research, 29, 249-266.
Govindaraju, K., 1994, Compilation of working values and descriptions for 383 Geostandards: Geostandard, Newsletter, 18, 1-158.
Gromet, L.P., Dymek, R.F., Haskin, L.A., Korotev, R.L., 1984, The "North American shale composite": Its compilation, major and trace elements characteristics: Geochimica et Cosmochimica Acta, 48, 2469-2482.
Gupta, S., Banerjee, R., Babu, P.V.R., Parihar, P.S., Maithani, P.B., 2012, Geochemistry of Uraniferous Banganapalle Sediments in the western part of Palnad Sub-basin, Andhra Pradesh: implications on Provenance and Paleo-weathering: Gondwana Geological Magazine Special Volume, 13, 1-14.
Hatch, J.R., Leventhal, J.S., 1992, Relationship between inferred redox potential of the depositional environment and geochemistry of the Upper Pennsylvanian (Missourian) Stark shale member of the Dennis Limestone, Wabaunsee County, Kansas, USA: Chemical Geology, 99, 65-82.
Hayashi, K.I., Fujisawa, H., Holland, H.D., Ohmoto, H., 1997, Geochemistry of ~1.9 Ga sedimentary rocks from northeastern Labrador, Canada: Geochimica et Cosmochimica Acta, 16, 4115-4137.
Jacques-Ayala, C., 1995, Paleogeography and provenance of the Lower Cretaceous Bisbee Group in the Caborca-Santa Ana area, northwestern Sonora, *in* Jacques-Ayala, C., González-León, C.M., Roldan-Quintana, J. (eds.), Studies on the Mesozoic of Sonora and adjacent areas: Geological Society of America Special Paper, 301, 79-98.
Jones, B., Manning, D.C., 1994, Comparison of geochemical indices used for the interpretation of paleo-redox conditions in Ancient mudstones: Chemical Geology, 111, 111-129.
Klinkhammer, G.P., Palmer, M.R., 1991, Uranium in the oceans: where it goes and why: Geochimica et Cosmochimica Acta, 55, 1799-1806.
Kübler, B., Jaboyedoff, M., 2000, Illite Cristallinity: Comptes Rendus de l'Académie des Sciences, Paris, 331, 75-89.
Lachance, G.R., Traill, R.J., 1966, A practical solution to the matrix problem in X-ray analysis, I. Method: Canadian Spectroscopy, 11, 43-48.
Lawton, T.F., González-León, C.M., Lucas, S.G., Scott, R.W., 2004, Stratigraphy and sedimentology of the Upper Aptian-upper Albian Mural Limestone (Bisbee Group) in northern Sonora, Mexico: Cretaceous Research, 25, 43-60.
Le Bas, M.J., Le Maitre, R.W., Streckeisen, A., Zanettin, B., 1986, A chemical classification of volcanic rocks based on the total alkali-silica diagram: Journal of Petrology, 27, 745-750.
Leung, K.W., Lai, C.Y., 1965, A synthesis of the genesis of reddish brown latosols in Taiwan: Journal of the Agricultural Association of China, New Series, 52, 81-102.
Mack, G.H., Kolins, W.B., Galemore, J.A., 1986, Lower Cretaceous stratigraphy, depositional environments, and sediment dispersal in southwestern New Mexico: American Journal of Science, 286, 309-321.
Madhavaraju, J., 2015, Geochemistry of Campanian-Maastrichtian sedimentary rocks in the Cauvery Basin, South India: Constrains on paleoweathering, provenance and Cretaceous environments, *in* Ramkumar, M. (ed.), Chemostratigraphy: Concepts, Techniques and Applications: Elsevier Special Volume, 185-214.
Madhavaraju, J., González-León, C.M., 2012, Depositional conditions and source of rare earth elements in carbonate strata of the Aptian-Albian Mural Formation, Pitaycachi section, northeastern Sonora, Mexico: Revista Mexicana de Ciencias Geológicas, 29, 478-491.
Madhavaraju, J., Lee, Y.I., 2009, Geochemistry of the Dalmiapuram Formation of the Uttatur Group (Early Cretaceous), Cauvery basin, southeastern

India: Implications on provenance and paleo-redox conditions: Revista Mexicana de Ciencias Geológicas, 26, 380-394.

Madhavaraju, J., Lee, Y.I., 2010, Influence of Deccan Volcanism in the sedimentary rocks of Late Maastrichtian-Danian age of Cauvery Basin, Southeastern India: Constraints from Geochemistry: Current Science, 98, 528-537.

Madhavaraju, J., Ramasamy, S., 1999, Rare earth elements in limestones of Kallankurichchi Formation of Ariyalur Group, Tiruchirapalli Cretaceous, Tamil Nadu: Journal of the Geological Society of India, 54, 291-301.

Madhavaraju, J., Ramasamy, S., 2001, Clay mineral assemblages and rare earth element distribution in the sediments of Ariyalur Group, Tiruchirapalli District, Tamil Nadu - Implication for Paleoclimate: Journal of the Geological Society of India, 58, 69-77.

Madhavaraju, J., Ramasamy, S., Ruffell, A., Mohan, S.P., 2002, Clay mineralogy of the Late Cretaceous and Early Tertiary successions of the Cauvery Basin (southeastern India): Implication for sediment source and Palaeoclimates at the K/T boundary: Cretaceous Research, 23, 53-163.

Madhavaraju, J., González-León, C.M., Yong Il Lee, Armstrong-Altrin, J.S., Reyes-Campero, L.M., 2010, Geochemistry of the Mural Formation (Aptian-Albian) of the Bisbee Group, Northern Sonora, Mexico: Cretaceous Research, 31, 400-414.

Madhavaraju, J., Sial, A.N., González-León, C.M., Nagarajan, R., 2013a, Carbon and oxygen isotopic variations in early Albian limestone facies of the Mural Formation, Pitaycachi section, northeastern Sonora, Mexico: Revista Mexicana de Ciencias Geológicas, 30, 526-539.

Madhavaraju, J., Yong IL Lee, González-León, C.M., 2013b, Diagenetic significance of carbon, oxygen and strontium isotopic compositions in the Aptian-Albian Mural Formation in Cerro Pimas area, northern Sonora, Mexico: Journal of Iberian Geology, 39, 73-88.

Madhavaraju, J., Hussain, S.M., Ugeswari, J., Nagarajan, R., Ramasamy, S., and Mahalakshmi, S., 2015a, Paleo-redox conditions of the Albian-Danian carbonate rocks of the Cauvery Basin, South India: Implications for Chemostratigraphy, *in* Ramkumar, M. (ed.), Chemostratigraphy: Concepts, Techniques and Applications: Elsevier Special Volume, 247-271.

Madhavaraju, J., Scott, R.W., Lee, Y.I., Bincy, K.S., González-León, C.M., Ramasamy, S., 2015b, Facies, biostratigraphy, diagenesis, and depositional environments of Lower Cretaceous strata, Sierra San José section, Sonora (Mexico): Carnets de Géologie (Notebooks on Geology), 15, 103-122.

Madhavaraju, J., Loser, H., Lee, Y.I., Lozano-Santacruz, R., Pi-Puig, T., 2016, Geochemistry of Lower Cretaceous limestones of the Alisitos Formation, Baja California, Mexico: Implications for REE source and paleo-redox conditions: Journal of South American Earth Sciences, 66, 149-165.

Mangini, A., Jung, M., Laukenmann, S., 2001,What do we learn from peaks of uranium and of manganese in deep sea sediments?: Marine Geology, 177, 63-78.

McLennan, S.M., 1993, Weathering and global denudation: The Journal of Geology, 101, 295-303.

McLennan, S.M., Hemming, S., McDaniel, D.K., Hanson, G.N., 1993, Geochemical approaches to sedimentation, provenance, and tectonics *in* Johnsson, M.J., Basu, A. (eds.), Processes controlling the composition of clastic sediments: Geological Society of America Special Paper, 284, 21-40.

Meyers, P.A., 1989, Sources and deposition of organic matter in Cretaceous passive margin deep-sea sediments: a synthesis of organic geochemical studies from Deep Sea Drilling Project Site 603, outer Hatteras Rise: Marine and Petroleum Geology, 6, 182-189.

Meyers, P.A., 1994, Preservation of elemental and isotopic source identification of sedimentary organic matter: Chemical Geology, 114, 289-302.

Meyers, P., Bernasconi, S.M., Forster, A., 2006, Origins and accumulation of organic matter in expanded Albian to Santonian black shale sequences on the Demerara Rise, South American margin: Organic Geochemistry, 37, 1816-1830.

Millot, G., 1970, Geology of clays: Berlin, Springer-Verlag, 499 pp.

Mondal, M.E.A., Wani, H., Mondal, B., 2012, Geochemical signature of provenance, tectonics and chemical weathering in the Quaternary flood plain sediments of the Hindon River, Gangetic plain, India: Tectonophysics, 566, 87-94.

Moore, D.M., Reynolds, R.C., 1989, X-ray Diffraction and the Identification and Analysis of Clay Mineral: Oxford, Oxford University Press, 378 pp.

Moosavirad, S.M., Janardhana, M.R., Sethumadhav, M.S., Narasimha, K.N.P., 2012, Geochemistry of Lower Jurassic sandstones of Shemshak Formation, Kerman Basin, Central Iran: provenance, source weathering and tectonic setting: Journal of the Geological Society of India, 79, 483-496.

Nagarajan, R., Madhavaraju, J., Nagendra, R., Armstrong-Altrin, J. S., Moutte, J., 2007a, Geochemistry of Neoproterozoic shales of the Rabanpalli Formation, Bhima Basin, Northern Karnataka, southern India: implications for provenance and paleoredox conditions: Revista Mexicana de Ciencias Geológicas, 24, 150-160.

Nagarajan, R., Armstrong-Altrin, J.S., Nagendra, R., Madhavaraju, J., Moutte, J., 2007b, Petrography and geochemistry of terrigenous sedimentary rocks in the Neoproterozoic Rabanpalli Formation, Bhima Basin, southern India: implications for paleoweathering condition, provenance, and source rock composition: Journal of the Geological Society of India, 70, 297-312.

Nath, B.N., Bau, M., Rao, R.B., Rao, Ch.M., 1997, Trace and rare earth elemental variation in Arabian Sea sediments through a transect across the oxygen minimum zone: Geochimica et Cosmochimica Acta, 61, 2375-2388.

Nesbitt, H.W., Young, G.M., 1982, Early Proterozoic climates and plate motions inferred from major element chemistry of lutites: Nature, 299, 715-717.

Nesbitt, H.W., Young, G.M., 1984, Prediction of some weathering trends of plutonic and volcanic rocks based on thermodynamic and kinetic considerations: Journal of Geology, 48, 1523-1534.

Nesbitt, H.W., Young, G.M., 1989, Formation and diagenesis of weathering profiles: Journal of Geology, 97, 129-147.

Nesbitt, H.W., Markovics, G., Price, R.C., 1980, Chemical processes affecting alkalies and alkaline earths during continental weathering: Geochimica et Cosmochimica Acta, 44, 1659-1666.

Nijenhuis, I.A., Bosch, H.J., Sinninghe-Damste, J.S., Brumsack, H.J., De Lange, G.J., 1999, Organic matter and trace element rich sapropels and black shales: a geochemical comparison: Earth and Planetary Science Letters, 169, 277-290.

Ramachandran, A., Madhavaraju, J., Ramasamy, S., Lee, Y.I., Rao, S., Chawngthu, D.L., Velmurugan, K., 2016, Geochemistry of the Proterozoic clastic rocks of Kerur Formation of Kaladgi-Badami Basin, Northern Karnataka, South India: Implications for paleoweathering and provenance: Turkish Journal of Earth Sciences, 25, doi:10.3906/yer-1503-4.

Ramírez-Montoya, E.G., 2014, Análisis geoquímico en la lutita de la Caliza Mural, Sección Tuape, para determinar procedencia, condiciones de oxigenación y paleointemperismo: Hermosillo, Sonora, Universidad de Sonora, tesis de licenciaturaa, 85 pp.

Ransome, F.L., 1904, The geology and ore deposits of the Bisbee quadrangle Arizona: United States Geological Survey Professional Paper, 21, 167 p.

Rau, G.H., Arthur, M.A., Dean, W.E., 1987, 15N/14N variations in Cretaceous Atlantic sedimentary sequences; implication for past changes in marine nitrogen biogeochemistry: Earth and Planetary Science Letters, 82, 269-279.

Raucsik, B., Varga, A., 2008, Climate-environmental controls on clay mineralogy of the Hettangian-Bajocian successions of the Mecsek Mountains, Hungary: An evidence for extreme continental weathering during the early Toarcian oceanic anoxic event: Palaeogeography Palaeoclimatology Palaeoecology, 265, 1-13.

Raza, M., Ahmad, A.H.M., Khan, M.S., Khan, F., 2012, Geochemistry and detrital modes of Proterozoic sedimentary rocks, Bayana Basin, north Delhi fold belt: implications for provenance and source-area weathering: International Geology Review, 54, 111-129.

Rimmer, S.M., 2004, Geochemical paleoredox indicators in Devonian–Mississippian black shales, Central Appalachian Basin (USA): Chemical Geology, 206, 373-391.

Roddaz, M., Viers, J., Brusset, S., Baby, P., Boucayrand, C., Herail, G., 2006, Controls on weathering and provenance in the Amazonian foreland basin: insights from major and trace element geochemistry of Neogene Amazonian sediments: Chemical Geology, 226, 31-65.

Roser, B.P., Korsch, R.J., 1988, Provenance signatures of sandstone-mudstone suites determined using discriminant function analysis of major element data: Chemical Geology, 67, 119-139.

Ruffell, A.H., Batten, D.J., 1990, The Barremian–Aptian arid phase in western Europe: Palaeogeography Palaeoclimatology Palaeoecology, 80, 197-212.

Ruffell, A.H., McKinley, J.M., Worden, R.H., 2002, Comparison of clay mineral stratigraphy to other proxy palaeoclimate indicators in the Mesozoic of NW Europe: Philosophical Transactions of the Royal Society, 360, 675-693.

Santoyo, E., Verma, S.P., 2003, Determination of lanthanides in synthetic standards by reversed-phase high performance liquid chromatography with the aid of a weighted least-squares regression model: estimation of method sensitivities and detection limits: Journal of Chromatography, 997, 171-182.

Sarkar, A., Bhattacharya, S.K., Sarin, M.M., 1993, Geochemical evidence for anoxic deep sea water in the Arabian Sea during the last glaciations: Geochimica et Cosmochimica Acta, 57, 1009-1016.

Scott, R.W., 1987, Stratigraphy and correlation of the Cretaceous Mural Limestone, Arizona and Sonora *in* Dickinson, W.R., Klute, M.F. (eds.), Mesozoic rocks of Southern Arizona and adjacent areas: Arizona Geological Society Digest, 18, 327-334.

Selvaraj, K., Chen, C.T.A., 2006, Moderate chemical weathering of subtropical Taiwan: Constraints from solid-phase geochemistry of sediments and sedimentary rocks: Journal of Geology, 114, 101-116.

Somayajulu, B.L.K., Yadav, D.N., Sarin, M.M., 1994, Recent sedimentary records from the Arabian sea: Proceedings of Indian Academy of Science, Earth and Planetary Science, 103, 315-327.

Spalletti, L.A., Limarino, C.O., Pinol, F.C., 2012, Petrology and geochemistry of Carboniferous siliciclastics from the Argentine Frontal Cordillera: A test of methods for interpreting provenance and tectonic Setting: Journal of South America Earth Science, 36, 32-54.

Srivastava, A.K., Randive, K.R., Khare, N., 2013, Mineralogical and geochemical studies of glacial sediments from Schirmacher Oasis, East Antarctica: Quaternary International, 292, 205-216.

Sun, Y., Puttmann, W., 1997, Metal accumulation during and after deposition of the Kupferschiefer from the Sangerhausen Basin, Germany: Applied Geochemistry, 12, 577-592.

Taylor, S.R., McLennan, S.M., 1985, The Continental Crust: its Composition and Evolution: Oxford, Blackwell, 349 pp.

Tribovillard N., Riboulleau A., Lyons T., Baudin, F., 2004, Enhanced trapping of molybdenum by sulfurized marine organic matter of marine origin in Mesozoic limestones and shales: Chemical Geology, 213, 385-401.

Tribovillard, N., Algeo, T.J., Lyons, T., Riboulleau, A., 2006, Trace metals as paleo-redox and paleo-productivity proxies: An update: Chemical Geology, 232, 12-32.

Újvári, G., Varga, A., Balogh-Brunstad, Z.S., 2008, Origin, weathering, and geochemical composition of loess in southwestern Hungary: Quaternary Research, 69, 421-437.

Újvarí, G., Varga, A., Raucsik, B., Kovács, J., 2013, The Paks loess-paleosol sequence: a record of chemical weathering and provenance for the last 800 ka in the mid-Carpathian Basin: Quaternary International, http://dx.doi.org/10.1016/j.quaint.2012.04.004.

Van Mooy, B.A.S., Keil, R.G., Devol, A.H., 2002, Impact of suboxia on sinking particulate organic carbon: enhanced carbon flux and preferential degradation of amino acids via denitrification: Geochimica et Cosmochimica Acta, 66, 457-465.

Verardo, D.J., MacIntyre, A., 1994, Production and preservation: control of biogenous sedimentation in the tropical Atlantic 0-300,000 years B.P: Paleoceanography, 9, 63-86.

Verma, S.P., Santoyo, E., 2005, Is odd-even effect reflected in detection limits?: Accreditation and Quality Assurance, 10, 144-148.

Verma, S.P., Santoyo, E., Velasco-Tapia, F., 2002, Statistical evaluation of analytical methods for the determination of rare-earth elements in geological materials and implications for detection limits: International Geology Review, 44, 287-335.

Vine, J.D., Tourtelot, E.B., 1970, Geochemistry of black shale deposits—A summary report: Economic Geology, 65, 253-272.

Wang, H.M., Chen, S.H., 1988, Mineralogical and chemical studies of gravel weathering and its relation to lateritic soil formation in the Linkou terrace: Tih-Chih, 8, 27-47.

Warning B., Brumsack H.J., 2000, Trace metal signatures of eastern Mediterranean sapropels: Palaeogeography Palaeoclimatology Palaeoecology, 158, 293-309

Weaver, C.E., 1989, Clays, Muds, and Shales: Amsterdam, Elsevier, 819 pp.

Wedepohl, K.H., 1971, Environmental influences on the chemical composition of shales and clays. *in* Ahrens, L.H., Press, F., Runcorn, S.K., Urey, H.C., (eds.) Physics and Chemistry of the Earth, 8: Oxford, Pergamon, 307-331.

Wedepohl, K.H., 1991, The composition of the upper earth's crust and natural cycles of selected metals. Metals in natural raw materials, Natural Resources, *in* Merian, E. (ed.), Metals and their compounds in the environment: VCH, Weinheim, 3-17.

Westermann, S., Duchamp-Alphonse, S., Fiet, N., Fleitmann, D., Matera, V., Adatte, T., Follmi, K.B., 2013, Paleoenvironmental changes during the Valanginian: New insights from variations in phosphorous contents and bulk-and clay mineralogies in th western Tethys: Paleogeography Paleoclimatology Paleoecology, 392, 196-208.

Wignall, P.B., Myers, K.J., 1988, Interpreting the benthic oxygen levels in mudrocks, a new approach: Geology, 16, 452-455.

Wilde, P., Lyons, T.W., Quinby-Hunt, M.S., 2004, Organic carbon proxies in black shales: molybdenum: Chemical Geology, 206, 167-176.

Wronkiewicz, D.J., Condie, K.C., 1987, Geochemistry of Archean shales from the Witwatersrand Supergroup, South Africa: source-area weathering and provenance: Geochimica et Cosmochimica Acta, 51, 2401-2416.

Yarincik, K.M., Murray, R.W., Lyons, T.W., Peterson, L.C., Haug, G.H., 2000, Oxygenation history of bottom waters in the Cariaco Basin, Venezuela, over the past 578,000 years: results from redox-sensitive metals (Mo, V, Mn, and Fe): Paleoceanography, 15, 593-604

Zaid, S.M., 2012, Provenance, diagenesis, tectonic setting and geochemistry of Rudies sandstone (Lower Miocene), Warda Field, Gulf of Suez, Egypt: Journal of African Earth Sciences, 66-67, 56-71.

Manuscript received: June 18, 2015
Corrected manuscript received: November 16, 2015
Manuscript accepted: November 24, 2015